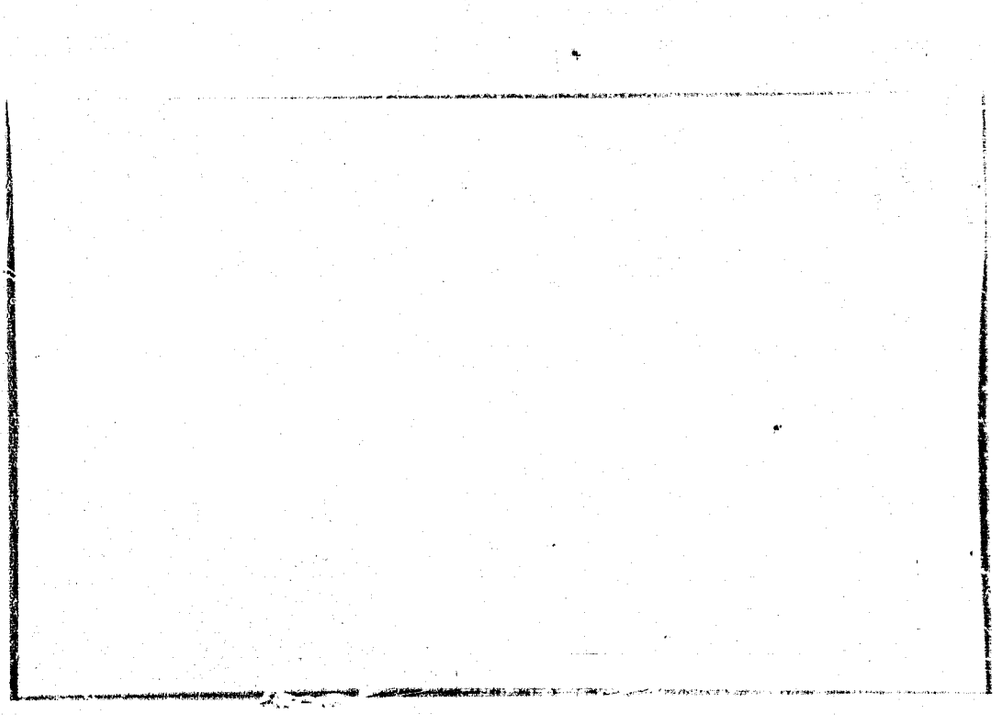

E S

ELECTRO-OPTICAL SYSTEMS, INC. Pasadena, California

Quarterly Report 17 May 1963 to 17 August 1963

DESIGN STUDY OF A SOLAR HYDROGEN PROPULSION AND POWER SYSTEM

Prepared for:

National Aeronautics and Space Administration
Office of Propulsion and Power Generation (Code-RP)
Washington 25, D.C.

Contract No. NAS 7-231
EOS Report 4000-Q-1

9 Sept. 1963

Prepared by

F. MacFarlane

Approved by

B. M. Wilner
Associate Manager
Energy Conversion Division

ELECTRO-OPTICAL SYSTEMS, INC. - PASADENA, CALIFORNIA

CONTENTS

		Page
1.	SUMMARY	1
2.	INTRODUCTION	2
3.	PERFORMANCE ANALYSIS OF COMPONENTS	5
	3.1 Propellant Storage and Feed System.	5
	3.1.1 Vented and Non-Vented Systems	5
	3.1.2 Propellant Storage and Feed System Geometry, and Structural Requirements.	9
	3.1.3 Insulation Requirements.	13
	3.1.4 Meteoroid Shielding	17
	3.2 Collector-Absorber Characteristics	21
	3.2.1 Collector-Absorber Efficiency	24
	3.3 Diode Characteristics.	37
	3.4 Thermal Energy Storage System.	40
4.	DESIGN STUDY OF COMBINED CAVITY ABSORBER	42
	4.1 Introduction	42
	4.2 Cavity Entrance, Flux Control, and Top Plate Considerations.	42
	4.3 Design Considerations for the Hydrogen Heat Transfer Coils	43
	4.4 Integration of the Thermionic Diodes.	46
	4.5 The Thermal Energy Storage System.	53
	4.6 The Hydrogen Diffusion Problem.	55
5.	MISSION STUDIES	55
	5.1 Introduction	55
	5.2 Analysis	56
	5.3 Conclusions	69

ILLUSTRATIONS

Figure		Page
3-1	Propellant Storage and Feed System	6
3-2	Temperature Entropy Diagram for Hydrogen Feed System	8
3-3	Tank Diameter vs. Surface Area	11
3-4	Total and Incremental Tank Weights vs Propellant Weight for Spherical Tank	12
3-5	Mean Temperature Difference vs Absorptivity/Emissivity	16
3-6	Rate of Occurrence of Punctures vs Shield Thickness	19
3-7	Required Beryllium Shield Thickness vs the Product of Exposed Surface Area and Exposure Time for Various Probabilities of Puncture	20
3-8	Shield Weight vs Propellant Weight	22
3-9	Paraboloid Reflector Cross-Section	23
3-10	Ratio of Re-Radiated or Reflected Radiation from Absorber to Solar Flux Incident on Absorber vs Ratio of Absorber Diameter to Sun's Image Diameter	25
3-11	Efficiency Definitions for SOHR-SET System	27
3-12	Mirror-Absorber Efficiency vs Ratio of Cavity Entrance Diameter to Sun's Image Diameter at 1 AU.	30
3-13	Mirror-Absorber Efficiency vs Cavity Temperature for Various Levels of Angular Surface Deviation.	32
3-14	Concentrator Diameter vs Weight	34
3-15	Mirror Diameter vs Thrust at 1 AU.	35
3-16	Mirror Diameter vs Power Available at 1 AU.	36
3-17	Thermionic Diode Performance vs Emitter Temperature	39
4-1	Integral SOHR-SET Cavity Design Concept	45
4-2	Modes of Heat Transfer from Cavity to Diode Emitter	47
4-3	Integral Regenerative and Radiation Cooled Diode Heat Rejection System.	51

Figure		Page
5-1	Hohmann Transfer Ellipse for Chemical Rocket	57
5-2	Coast Ellipse for SOHR-SET and Ion Engine	57
5-3	Time of Powered Flight vs Initial Thrust Acceleration	60
5-4	Distance from Sun at Instant of Thrust Termination vs Initial Thrust Acceleration	61
5-5	Power Plant Mass Fraction vs Initial Thrust Acceleration	62
5-6	Propellant Mass Fraction vs Initial Thrust Acceleration	63
5-7	Payload plus Structure Mass-Fraction vs Initial Thrust Acceleration	65
5-8	Total Mission Time vs Initial Thrust Acceleration	66
5-9	Period of Coast Ellipse vs Initial Thrust Acceleration	67
5-10	Aphelion Distance of Coast Ellipse vs Initial Thrust Acceleration	68

1. SUMMARY

The objectives of this program are to perform a design study of a solar-hydrogen propulsion and power system for space applications. The study was initiated on 17 May 1963 under Contract NAS 7-231, and is planned for completion over a period of six (6) months. This informal quarterly report covers the work performed during the first three (3) months of the program.

During the report period, most of the component studies were completed and relationships were formulated for the cryogenic storage system, solar concentrator size, thrust levels, electrical power, and efficiencies at different solar distances. Subsystem integration studies of the cavity with combined hydrogen heat exchanger and thermionic converter were initiated. Preliminary studies of the combined cavity-absorber indicate the feasibility of the concept; however, problem areas associated with temperature distribution, thermal energy storage, and materials compatibility will require additional evaluation. A preliminary analysis of the system for a solar probe mission was completed, and results indicate that the combined solar propulsion-power system may offer significant performance advantages over electric propulsion or chemical rockets for this application. These studies will be refined and completed during the remainder of the program, with primary emphasis on integrated cavity-absorber design studies.

During the report period approximately 1,032 manhours and $16,000 were expended.

2. INTRODUCTION

At the earth's mean distance from the sun the solar flux in space is 130 watts/ft^2, and as the sun is approached this value increases as the inverse of the square of the distance from the sun. It is therefore natural to examine ways of utilizing this energy, whenever energy sources are under consideration for space missions in the solar system. The ideal situation would be to convert solar radiation directly to electricity. Unfortunately, this is only possible to a limited extent. One of the most promising approaches is to convert solar energy directly into heat, then utilize the heat in an energy conversion device. The drawback here is that for reasonable efficiencies we are confronted with thermodynamic considerations requiring high temperatures, thus high temperature materials technology is necessary.

The sun's image is finite, hence the sun's image on the focal plane is finite. This fact, coupled with ever present mirror inaccuracies, spread the sun's image on the focal plane, and limit the maximum cavity temperature available. Hence, a high-precision mirror technology is necessary. Until recently, these advanced technologies were inadequate for engineering purposes.

The conversion of heat to electricity by thermionic diodes is capable of achieving an estimated maximum efficiency of 20-25 percent. Currently it is possible to engineer systems with about 10-15 percent efficiency. The remainder of the heat is normally dissipated. If a significant fraction of this wasted heat is utilized for preheating the hydrogen in a solar-hydrogen rocket (SOHR), the overall-system efficiency will be much better than that for the separate systems.

The SOHR propulsion system has four major components: the liquid hydrogen storage system, the solar collector, the cavity heat exchanger, and the rocket nozzle. Solar energy is concentrated by a light-weight all metal parabolic reflector which ranges in diameter from 5 to 40 feet depending upon the thrust needed for a particular mission.

The solar radiation is reflected into a cavity absorber with an aperture diameter of 1 percent of the collector diameter. This black body cavity encloses a refractory-metal heat exchanger through which hydrogen gas circulates. After it absorbs the heat, the gas is expanded through a nozzle. EOS has developed light-weight cavities which have operated at about 4500°R for extended durations. These cavities were fabricated from rhenium, molybdenum, and tungsten.

A prerequisite to the development of a useful solar-hydrogen rocket is the attainment of 3000 to 4000°R gas temperature exiting from a cavity (corresponding to 600-800 sec. specific impulse). Until recently neither the high temperature metals technology nor the necessary high precision mirrors were available. At present EOS builds 5-foot diameter mirrors with almost 90 percent mirror reflectivity and mirror to cavity aperture concentration ratios in excess of 10^4. These reflectors weigh approximately 0.5 pounds per square foot of projected area, and have a maximum deviation of the surface contour of less than 5 minutes. EOS is also fabricating elements of a high precision 40-foot diameter concentrator, and has recently demonstrated the feasibility of the solar hydrogen rocket propulsion concept on Contract No. AF 04 (611)-8181, with the operation of a ground demonstration model.

The thermionic diode is an electronic device for the conversion of heat directly into electricity. It is a device in which the cathode is raised to electron emission temperature by exposing the external surface of the cathode to the radiation of a high temperature heat source. The interelectrode gap is filled with low pressure cesium vapor for space charge neutralization so as to increase the energy available to an external load. Thermionic diodes at present have low

thermal efficiencies, hence in practice from five to ten times the electrical power delivered must be rejected as heat via the anode. The diodes deliver high current density at low voltage. A solar-energy thermionic (SET) power conversion device has been successfully built and operated by EOS under contract to the Jet Propulsion Laboratory (Contract No. JPL-950109). The generator produced a maximum of 45 watts--the largest power level achieved by such a device to date. Currently, EOS is building improved devices (JPL Contract 950349) to deliver 75 watts.

The present day SET generator rejects over ten times the equivalent electrical energy generated. Part of this waste heat can be saved if it is used to preheat the working fluid for a combined SOHR-SET device. Such devices, in larger sizes, could be made to produce several pounds thrust with many kilowatts of electrical output.

The SOHR-SET system envisioned will differ from the individual SOHR or SET systems only by the fact that there will be a common cavity with the diode emitter operating at a temperature slightly lower than the rest of the cavity. It should be capable of operation at varying distances from the sun. If desired, thermal energy storage can be incorporated for operating in the sun's shadow. It is expected to operate as a constant thrust device during thrusting, and at a constant power level.

3. PERFORMANCE ANALYSIS OF COMPONENTS

The SOHR-SET System is best suited to a class of missions intermediate between chemical and electric propulsion systems. Characteristic of the SOHR-SET system mission capabilities is low thrust, high specific impulse, and large payloads in low gravitational fields at the expense of flight time. Since the propulsion aspect requires the storage of large volumes of liquid, (the SOHR aspect of the system requires large mass fractions) then cryogenic storage considerations must be taken into account. Furthermore, since large areas are involved and long flight times are anticipated, micro-meteorite protection may become a significant factor.

3.1 Propellant Storage and Feed System.

The following sections deal with the analysis of the tankage weight required for typical SOHR-SET missions.

3.1.1 Vented and Non-vented Systems

The designer of a liquid hydrogen storage system for prolonged space missions must decide very early on the disposition of hydrogen boil off due to heat leakage into the system. If it is decided to vent the system to prevent excessive pressure build up, then the best that can be done is to optimize the boil-off-insulation relationship. For long duration missions the penalty is severe. Reference 1 gives an analysis of the boil-off penalties involved in a vented system. This study will be based on a non-vented system design concept.

In a non-vented system thermal leakage must be transferred from the body of the stored hydrogen to the exiting liquid. This can be done by throttling the hydrogen, then passing the wet mixture of liquid hydrogen droplets and saturated vapor through coils immersed in the storage tank. Figure 3-1 is a schematic of a non-vented system using stored gas pressurization. The system consists of the shield, tank plus suitable valves, regulators, expulsion bladder, throttling and warm-up coils, and other items. A schematic of the fuel tank wall is shown at the bottom of the page. The tank wall consists of the internal skin which contains the pressurized hydrogen, a layer of thermal insulation, a meteoroid shield, and a tank support structure.

The tank wall shown should not be considered as being the final form, since more optimized arrangements are possible. The interlacing of several layers of insulation and shielding is a distinct possibility as far as a lower weight design is concerned.

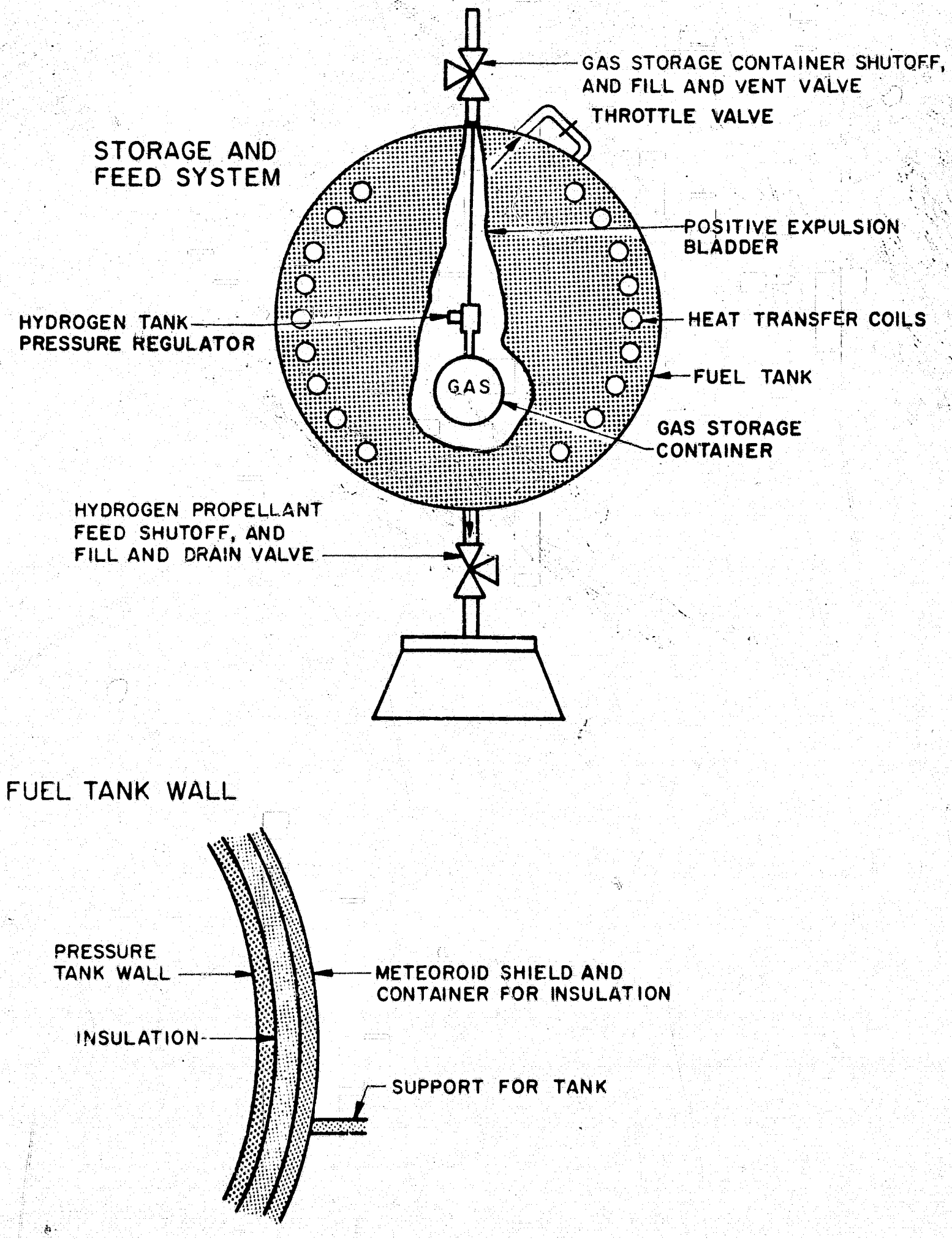

FIG. 3-1 PROPELLANT STORAGE AND FEED SYSTEM

However, no further consideration need be given to this problem until further knowledge is gained concerning the meteoroid environment, and the relative merits of one type of shield configuration over the other is determined.

Figure 3-2 is the Temperature-Entropy diagram for liquid hydrogen controlled vaporization. State 1 corresponds to the condition of bulk storage. The fluid is stored under saturated liquid condition at a pressure p_1, temperature T_1, and enthalpy h_1. At state 2, the fluid is throttled resulting in a decrease in pressure and temperature, and an increase in quality X_2. At state 3 the fluid is recirculated through the fuel tank where its enthalpy is increased to h_3, and its quality increased to X_3. At state 4 the fluid is throttled resulting in a decrease in pressure and temperature and an increase in quality from X_3 to the near saturated vapor. At state 5 the saturated vapor enters the first of a set of heat exchangers. Here it is warmed up sufficiently so that it can be handled easily in a flow control system. Another function of this heat exchanger is to make absolutely sure that no hydrogen droplets remain, thereby providing single phase vapor in the higher temperature exchangers.

The thermal leakage to the hydrogen will depend upon, among other things, the distance of the space craft from the sun. In actual practice we can anticipate several situations. We can envision the space-craft being on a mission so that at the end, it is closer to the sun than at any other point. We can also imagine this space-craft being further away from the sun at the end of the mission. There is the additional case in which space-craft is alternately close to and far removed from the sun, and finally, the craft may always be approximately the same distance from the sun. For the case in which the space-craft is closest to the sun at the end of the mission, the insulation must be adequate enough so that at the end of the mission the thermal leakage is not greater than the rate which enthalpy is being removed from the system by the existing hydrogen stream. This being the case the hydrogen

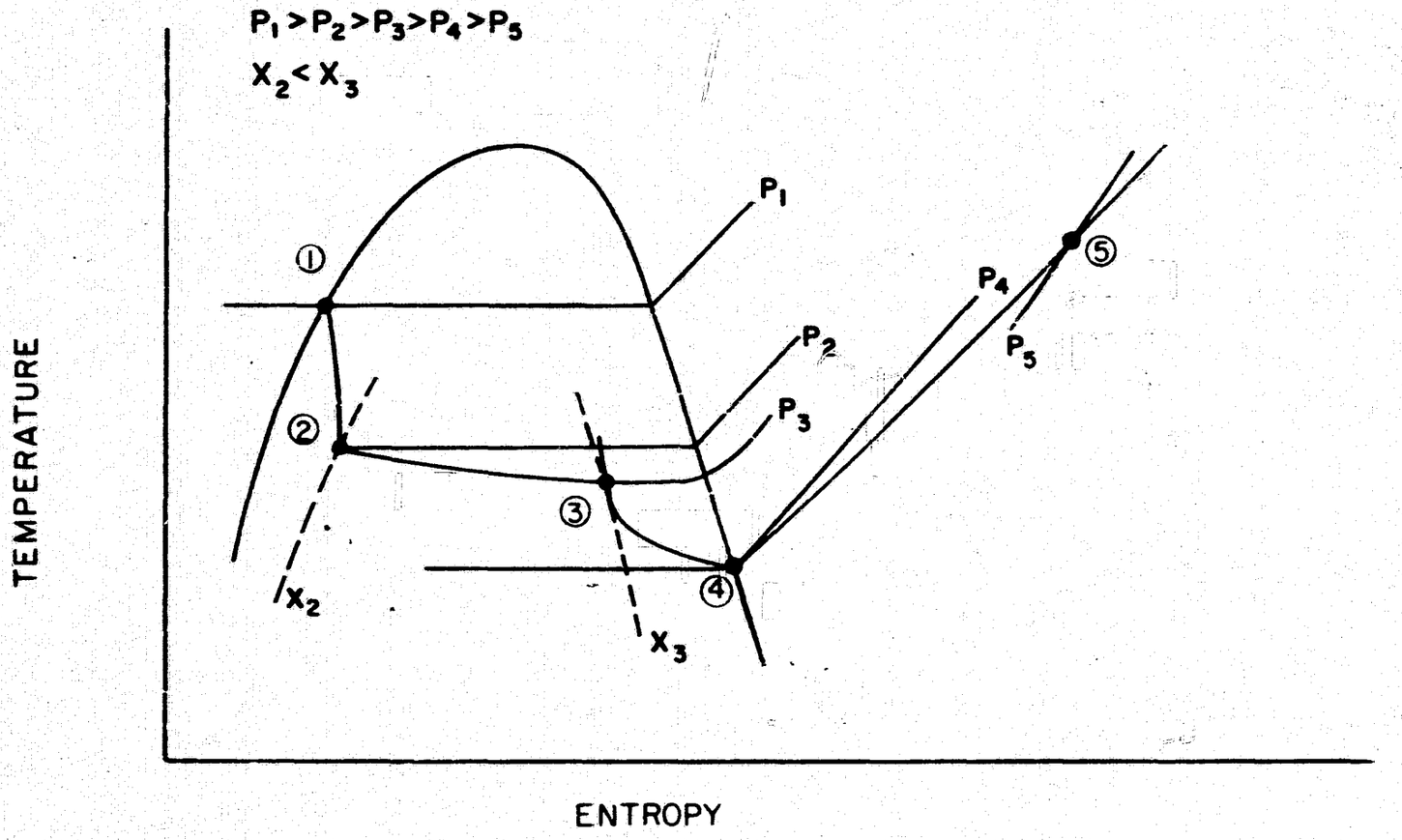

FIG. 3-2 TEMPERATURE ENTROPY DIAGRAM FOR HYDROGEN FEED SYSTEM

leaving the tank will always be of a quality less than 1, except at the end of the mission when its quality is 1, so that the first heat exchanger will in essence also be a vaporizer. For the case where the space vehicle is closest to the sun at the beginning of the mission, then the reverse case is true. Then again the first heat exchanger will also be a vaporizer. For the case where the space craft is alternately near and far removed from the sun, then the design must be for the point of closest approach to the sun, and for parts of the mission again the first heat exchanger will also be a vaporizer. The only missions on which the exiting hydrogen stream will be essentially a saturated vapor will be those in which the space craft distance from the sun remains approximately constant.

3.1.2 Propellant Storage and Feed System Geometry and Structural Requirements

The propellant storage and feed system weight consists of propellant weight plus the weight of the structure used to store and feed the propellant. The propellant weight consists of the hydrogen consumed for propulsion plus the propellant remaining after mission completion. The structure weight consists of pressure tank insulation and meteoroid shield. The pressure tank weight is derived partly from internal pressure considerations, and partly from other incremental factors described below. Since thermal insulation can serve as a meteoroid shield, and a meteoroid shield does have some thermal insulating properties, then the sum of the weights of thermal insulation and meteoroid shield should be optimized for a particular mission. In this analysis this has not been done.

As stated above $W_{sys} = W_{prop} + W_{struc}$

where W_{sys} = system weight

W_{prop} = propellant weight

W_{struc} = storage and feed system structure weight.

The make-up of the structure weight is as follows:

$$W_{struc} = W_v + W_i + W_m$$

where W_i = weight of the insulating layer

W_m = weight of the meteoroid shield

$$W_v = W_{press} + \Delta W_{ba} + \Delta W_{sa} + W_e + \Delta W_{sf}$$

The contributions to W_v are defined as follows:

W_{press} = theoretical weight of propellant tank due to internal gas pressure.

ΔW_{ba} = incremental weight of propellant tank due to boost phase acceleration.

ΔW_{sa} = the incremental weight of tank due to state of the arc restrictions in material gauges.

ΔW_e = incremental weight due to weight of expulsion bladder and associated structure of expulsion system (valves, regulators, etc.)

ΔW_{sf} = incremental weight due to factor of safety requirements.

The propellant tank geometry is arrived at by placing two constraints upon the over-all problem of propellant tank design. It is assumed that the tank has the minimum surface to volume ratio, and that it is adaptable to present booster vehicle systems.

The minimum area is necessary, not only to reduce the overall weight of the tank, but also to reduce the weight of meteoroid shielding, thermal insulation, and the necessary structural supports. Figure 3-3 shows the relationship between tank diameter (lbs. of liquid hydrogen) and the tank diameter and surface area.

Figure 3-4 shows the propellant tank weight for storage of liquid hydrogen at 50 psia using Ti-5Al-2.5 Sn alloy. Note that the upper curve W_v gives the propellant tank weight, whereas the lower curves are plots of the theoretical minimum value, and the incremental values.

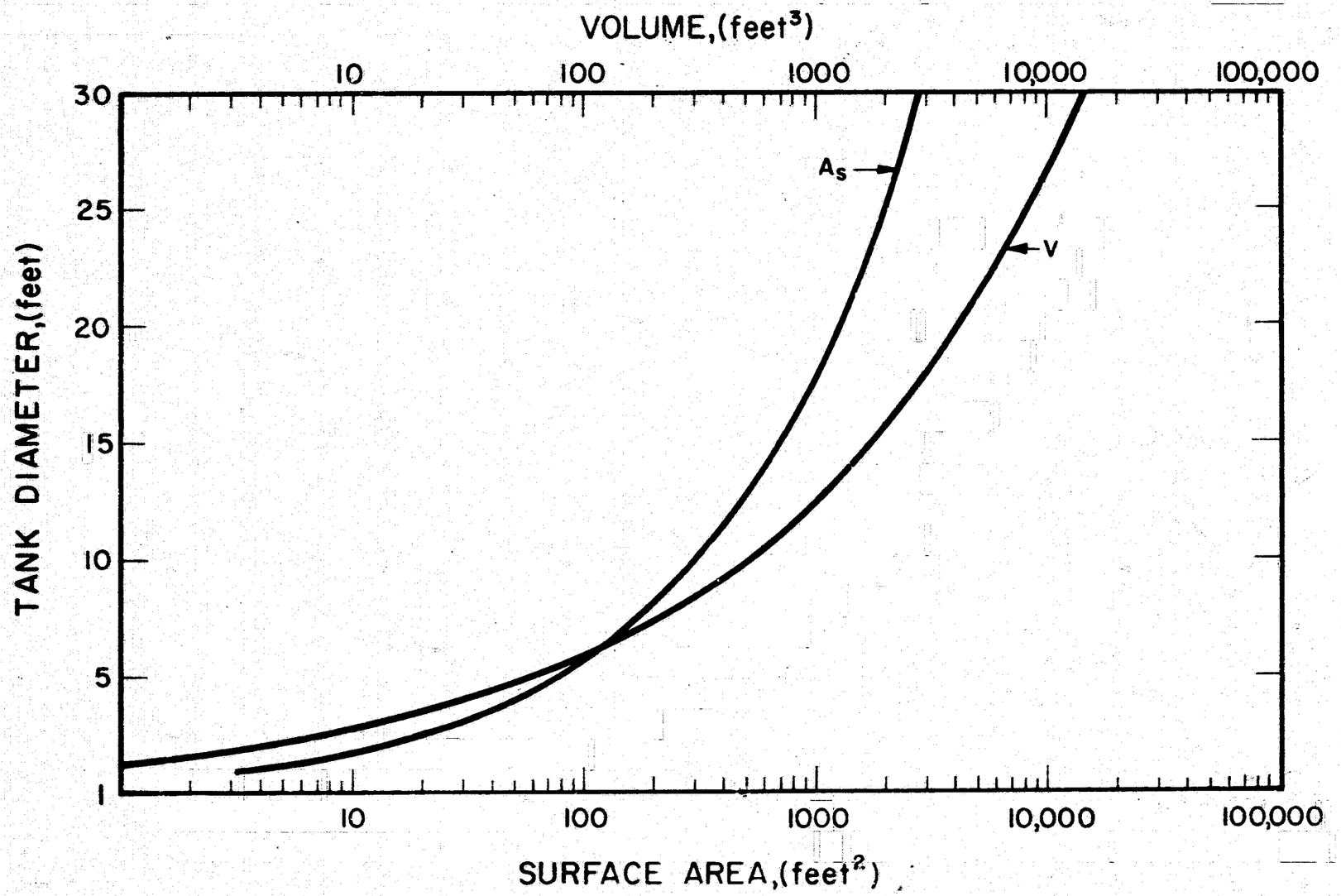

FIG. 3-3 TANK DIAMETER VS SURFACE AREA

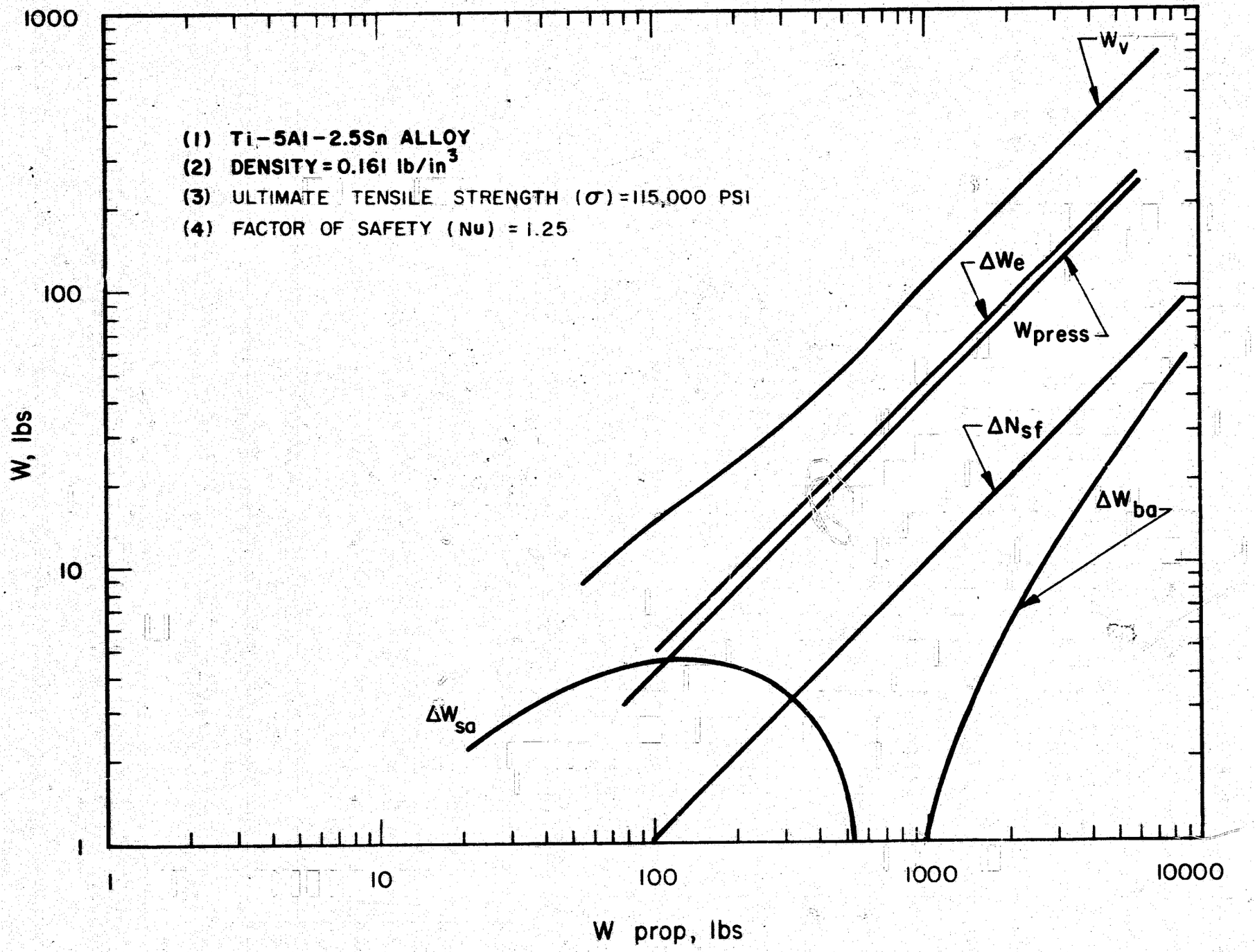

FIG. 3-4 TOTAL AND INCREMENTAL TANK WEIGHTS Vs PROPELLANT WEIGHT FOR SPHERICAL TANK

3.1.3 Insulation Requirements

The heat transferred to a space vehicle in a solar system depends on its location in space relative to the sun and the other planets, and also on its motion and orientation relative to them.

For the case of a non-venting system the propellant use rate is equal to the boil off rate at the point of closest approach of the space vehicle to the sun.

Let X = insulation thickness

T = temperature drop

k = thermal conductivity

A_s = surface area

F = thrust

D = mirror diameter

ρ = insulation density

Therefore, the heat input rate per unit area = $\frac{k \Delta T}{X}$

The total heat input is now

$$\int_{\text{surface}} \frac{k}{X} \Delta T \, dA_s$$

We will now define a mean temperature difference as equal to

$$\frac{\int \Delta T \, dA_s}{A_s}$$

Therefore, the total heat input rate is equal to

$$\frac{A_s K \Delta T_m}{X}$$

The boil off rate is equal to the total heat input rate divided by the heat of vaporization.

Hence boil off rate is equal to

$$\frac{A_s K \Delta T_m}{X H_v}$$

where H_v is the heat of vaporization of the liquid hydrogen. Let I_{sp} be the specific impulse of the hydrogen leaving the cavity. Therefore the use rate is equal to

$$\frac{F}{I_{sp}}$$

Equating the boil off rate to the use rate and noting that the insulation weight is equal to $\rho X A_s$ we find that the insulation weight is equal to

$$\frac{\rho A_s^2 K \Delta T_m I_{sp}}{H_v F}$$

Thermal conductivity values for evacuated laminated foil insulation have been reported as follows:

$k = .012\text{-}.05 \times 10^{-3}$ btu/hr-ft-^{o}R ,$(36^{o}\text{-}530^{o})$R

$\rho = 7.5$ lbs./ft.^{3}. To obtain high performance space vacuum conditions must be maintained between the many layers of aluminum foil, or aluminized mylar.

The mean temperature difference will now be estimated first for an orbit around the earth, and then for any point in space as a function of the distance from the sun. First we define the following terms:

Q_e = rate of thermal radiation emitted from an arbitrary element of tank surface.

Q_v = the rate of transmission of thermal leakage to the stored hydrogen.

Q_a = the rate at which radiation is being absorbed by arbitrary element of the tank surface. This radiation may be direct solar radiation emission radiation or reflected radiation.

ϵ_s = the surface emissivity of the tank.

σ = Stefan-Boltzman constant

T_s = tank surface temperature,

Taking a thermal balance about a tank element at temperature T_s, we find that

$$Q_a = Q_e + Q_v$$

Since the thermal leakage is much smaller than the emitted radiation from the tank surface, Q_v is much less than Q_e and $Q_a \approx Q_e$.

Therefore $Q_a \approx \epsilon_s \sigma T^4_s$. From this point on in, the analysis we will assume that all the radiation is solar radiation, and that the orientation of the space craft with respect to the sun is always the same. Figure 3-5 is a plot of the average temperature drop, versus the absorptivity-emissivity ratio of the space craft orbiting the earth. Curve 4 is applicable to our design since the SOHR-SET space craft must always be accurately focused on the sun, and also since any lateral thermal conductivity in the insulation can be assumed negligible. Over the range of low surface temperatures 0-600°R surface coatings composed of organic base white paints have achieved α/ϵ ratios of 0.2. Hence, a design point of ΔT_m of 160°F is reasonable for design conditions at one Astronomical Unit. (AU)

To estimate the variation of surface temperature with the distance to the sun we define

R = the distance of the space craft from the sun.

$$T_s \sim Q_a^{1/4}$$

Furthermore, we can assume that

$$Q_a \sim H$$

and $$H \sim 1/R^2$$

therefore, $$T_s \sim \left(1/R\right)^{1/2}$$

Now let the subscript 0 refer to conditions of one AU, and let the subscript 1 refer to conditions elsewhere.

Let

T_i = the temperature inside the storage tank

therefore, $\Delta T = T_s - T_i$

and $T_s = \Delta T + T_i$.

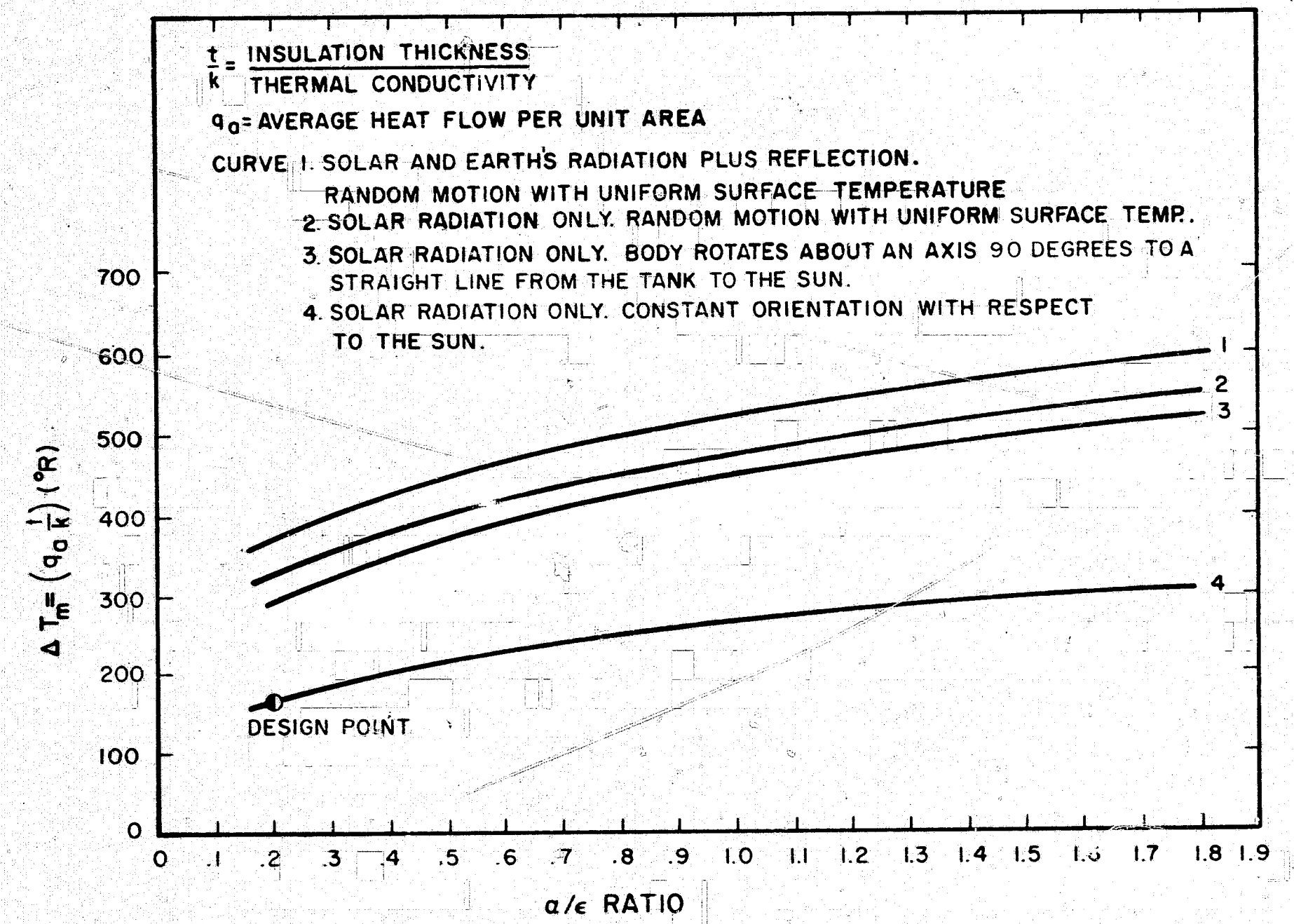

FIG. 3-3 MEAN TEMPERATURE DIFFERENCE VS $\frac{\text{ABSORPTIVITY}}{\text{EMISSIVITY}}$

Hence,

$$\left(\frac{\Delta T_1 + T_i}{\Delta T_o + T_i}\right) = \left(\frac{R_o}{R_1}\right)^{1/2}$$

and

$$\Delta T_1 = -T_i + \left(\frac{R_o}{R_1}\right)^{1/2} \left(\Delta T_o + T_i\right)$$

$$\Delta T_{m_1} \int_{\text{surface}} \frac{\Delta T_1 \, dA_s}{A_s}$$

thus

$$\Delta T_{m_1} = \int_{\text{surface}} \left[-T_i + \left(\frac{R_o}{R_1}\right)^{1/2} \left(\Delta T_o + T_i\right)\right] \frac{dA_s}{A_s}$$

This gives

$$\Delta T_{m_1} = -T_1 + \left[\left(\frac{R_o}{R_1}\right)^{1/2} \left[\Delta T_{m_0} + T_i\right]\right]$$

Combining this equation with the equation for insulation weight then

$$\text{Insulation weight} = \frac{A_s^2}{F} \left(\frac{K I_{sp} \rho}{H_v}\right) \left[-T_i + \left(\frac{R_o}{R_1}\right)^{1/2} \left(\Delta T_{m_o} + T_i\right)\right]$$

Hence, we can plot insulation weight versus $\frac{A_s^2}{F}$ with $\frac{R_o}{R_1}$ as parameter.

3.1.4 Meteoroid Shielding

Any vehicle operating in space for a prolonged period of time must be protected from meteoroid damage by a protective shield. Estimates of the meteoroid effects on the space structure depend on two sets of data, namely; the frequency with which the surface will be struck by a particle with a given size, velocity, direction, and composition, and the penetrating ability of a particle on a particular surface of a given thickness. Figure 3-5 gives penetration data for steel and aluminum as deduced from the works of Whipple and Bjork. Also included

in Figure 3-6 is penetration data based on the 1963 findings of Explorer XVI, reference 2. It should be noted that the Explorer XVI data were obtained only for penetrations of stainless steel material a few mils thick, and that extrapolation to material thickness of say 1/4 inch has yet to be verified. Note that the curve derived by assuming meteoroid densities of 0.5 gms. per cm.^{3} forms an upper boundary for recent Explorer XIV data.

The effectiveness of the optical surface of the solar concentrator, and of the surface coatings used for structures and for the thermal protection of propellant tanks will be affected by the average depth of the surface coating destroyed by meteoroids. Analysis has shown that much less than 1 percent of the mirror surface will be affected. For long periods of time meteoroid punctures follow a random arrival, or Poisson distribution. This assumption is used to calculate the meteoroid shield weight necessary for prolonged space craft operation. We define P(n) as the probability that n punctures of a sensitive area A will occur in a given time λ. Assume that the shielding material is beryllium of density 0.066 lbs. per inch.^{3} From Figure 3-6, we can find the expected value of the number of punctures for any area or for a given time.

Ψ = number of punctures/m^2-sec

A = exposed area, m^2

λ = exposure time, sec.

t = thickness in mils

the expected value of the number of punctures is $\Psi A\lambda$, hence P(n) and P(0) = exp-($\Psi A\lambda$) are known. Since $\Psi_{beryllium} = 1.45 \times \Psi_{steel}$, the shield thickness for beryllium is expressed by

$$t = 23.5 \frac{A\lambda}{1-P(0)}$$

for values of P (0) $\geq$0.90.

Figure 3-7 is the plot of the beryllium shield thickness required for preventing meteoroid penetrations, as a function of time. The required shield thickness based on Whipple's data, is approximately three times greater than the thickness based on Explorer XVI data.

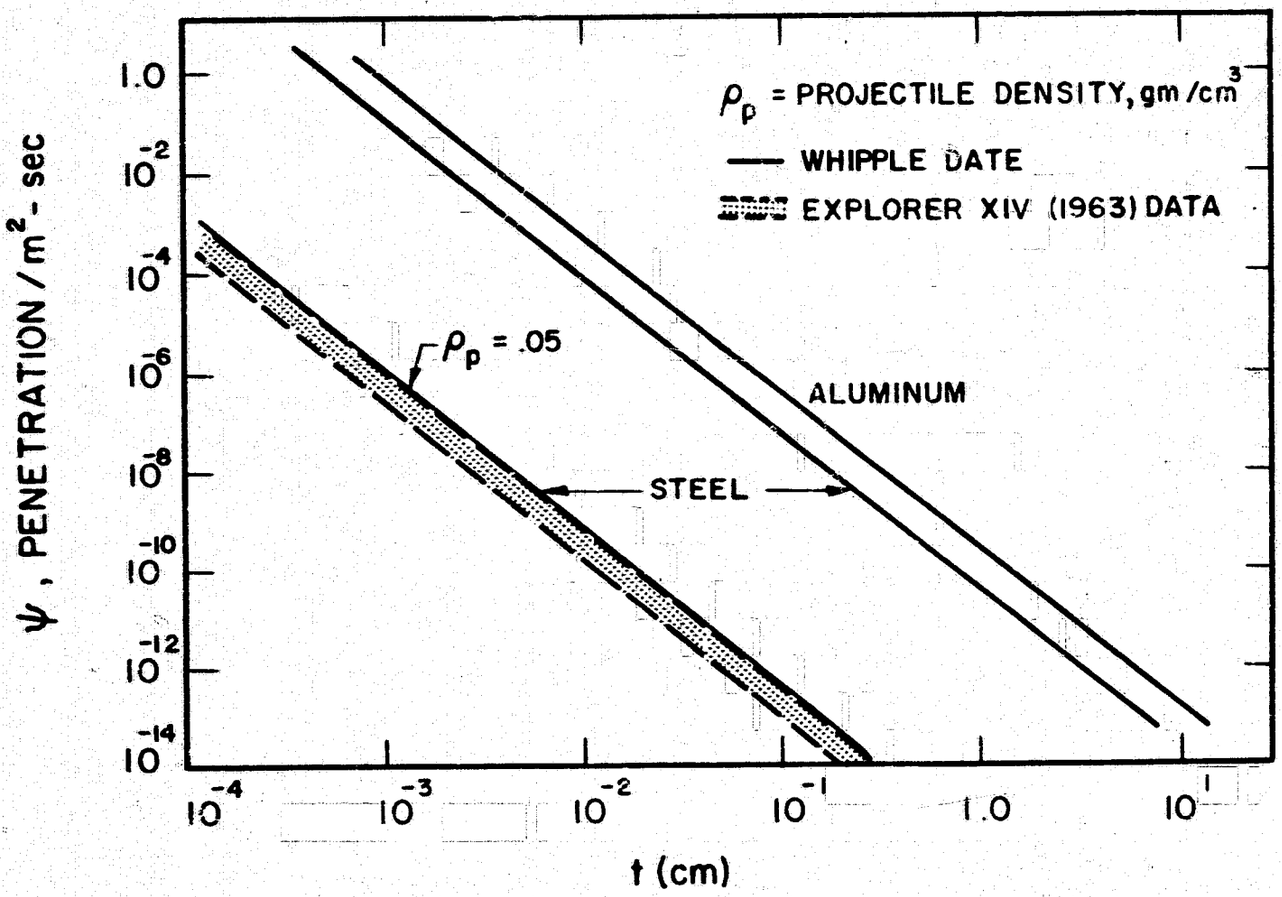

FIG. 3-6 RATE OF OCCURRENCE OF PUNCTURES VS SHIELD THICKNESS

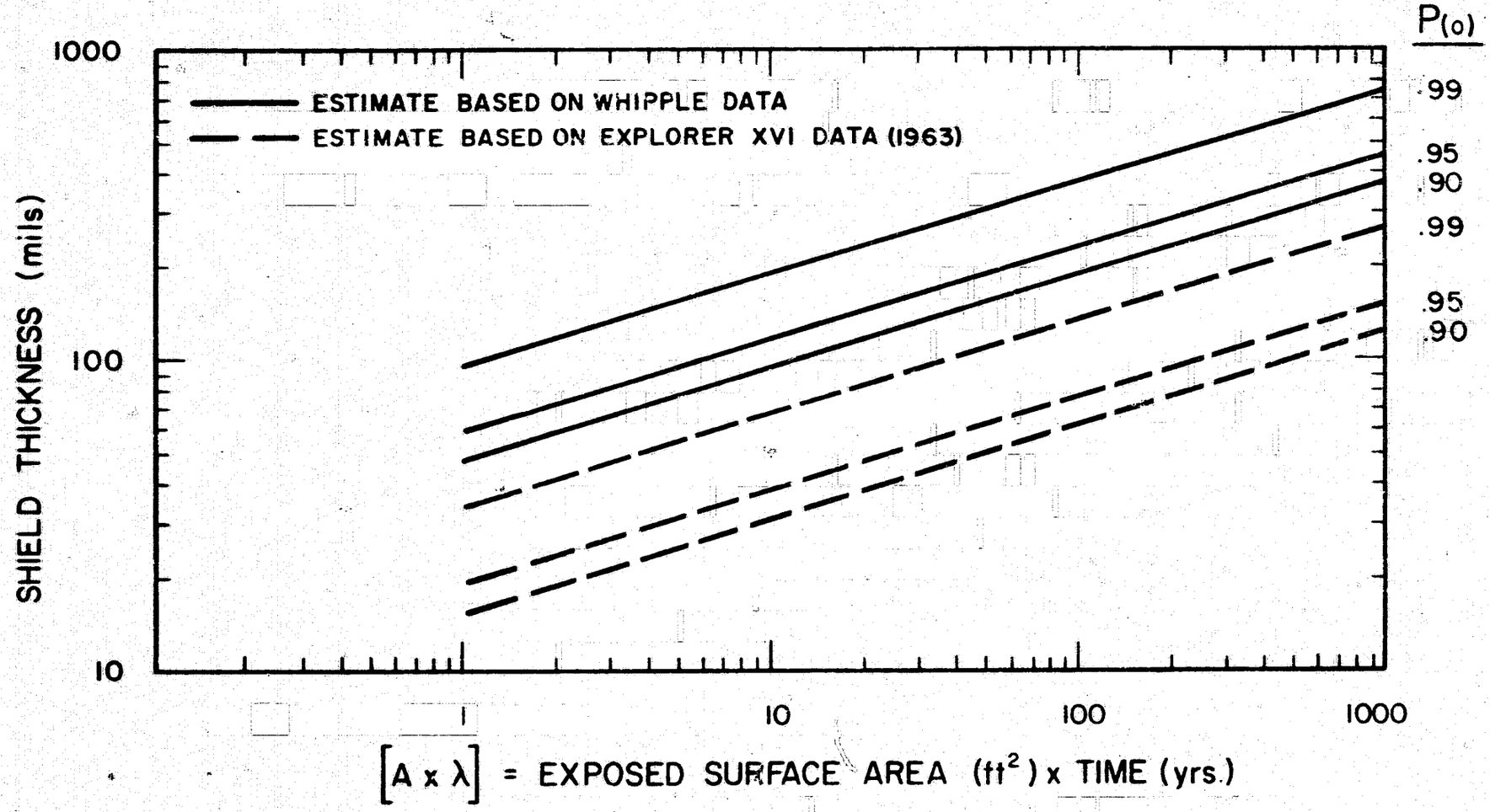

FIG. 3-7 REQUIRED BERYLLIUM SHIELD THICKNESS VS THE PRODUCT OF EXPOSED SURFACE AREA AND EXPOSURE TIME FOR VARIOUS PROBABILITIES OF PUNCTURE

Figure 3-8 gives a shielding requirement for various quantities of stored hydrogen. The shielding figures are based on the tank configuration discussed previously.

The results indicate that for a 90 percent survival probability of no penetrations, the meteoroid shield requirement based on the Explorer XVI data will be only about 6 percent of the propellant weight for a 100 day mission, and about 3 percent of propellant weight for a 10 day mission. Of course, if the design is based upon the earlier Whipple data, then the figures would be approximately three times larger.

3.2 Collector-Absorber Characteristics

The paraboloidal reflector is without question the logical selection for the high-temperature SOHR-SET application. It is the only concentrator that allows the attainment of high temperatures at high efficiency. Figure 3-9 illustrates the cross section of a paraboloid reflector, as well as the shape of a theoretically ideal focal image.

The parameters of interest in the selection of a specific paraboloid concentrator are summarized below. Each parameter is closely linked to the others, and each must be considered in a final selection.

1. Geometry
   a. Diameter
   b. Focal length
2. Accuracy
   a. Angular and linear surface deviations from true paraboloid.
   b. Figure distortion
3. Physical characteristics
   a. Weight
   b. Type of fabrication techniques
   c. Folded volume
   d. Support members
   e. Unfolding mechanisms

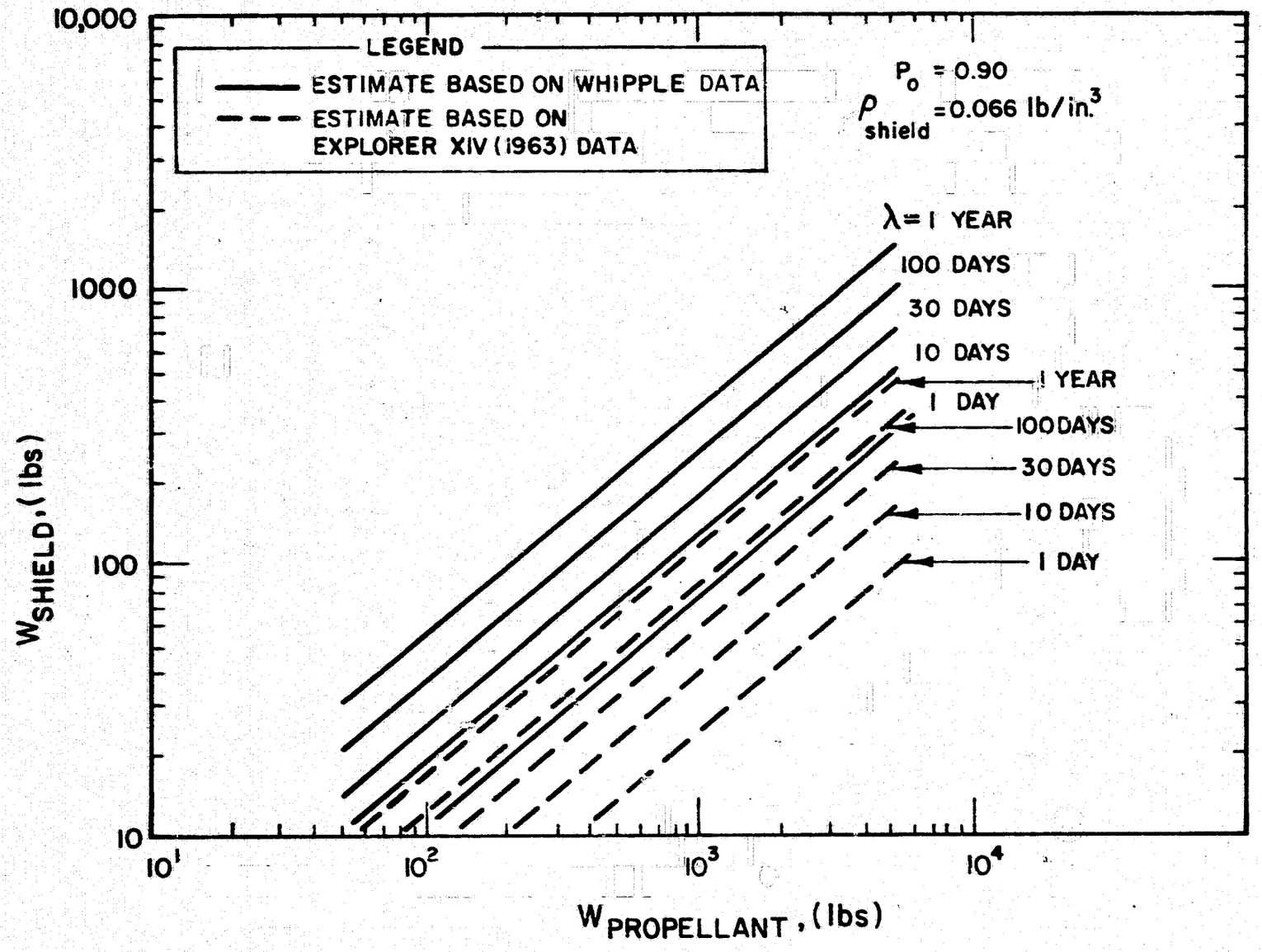

FIG. 3-2 SHIELD WEIGHT VS PROPELLANT WEIGHT

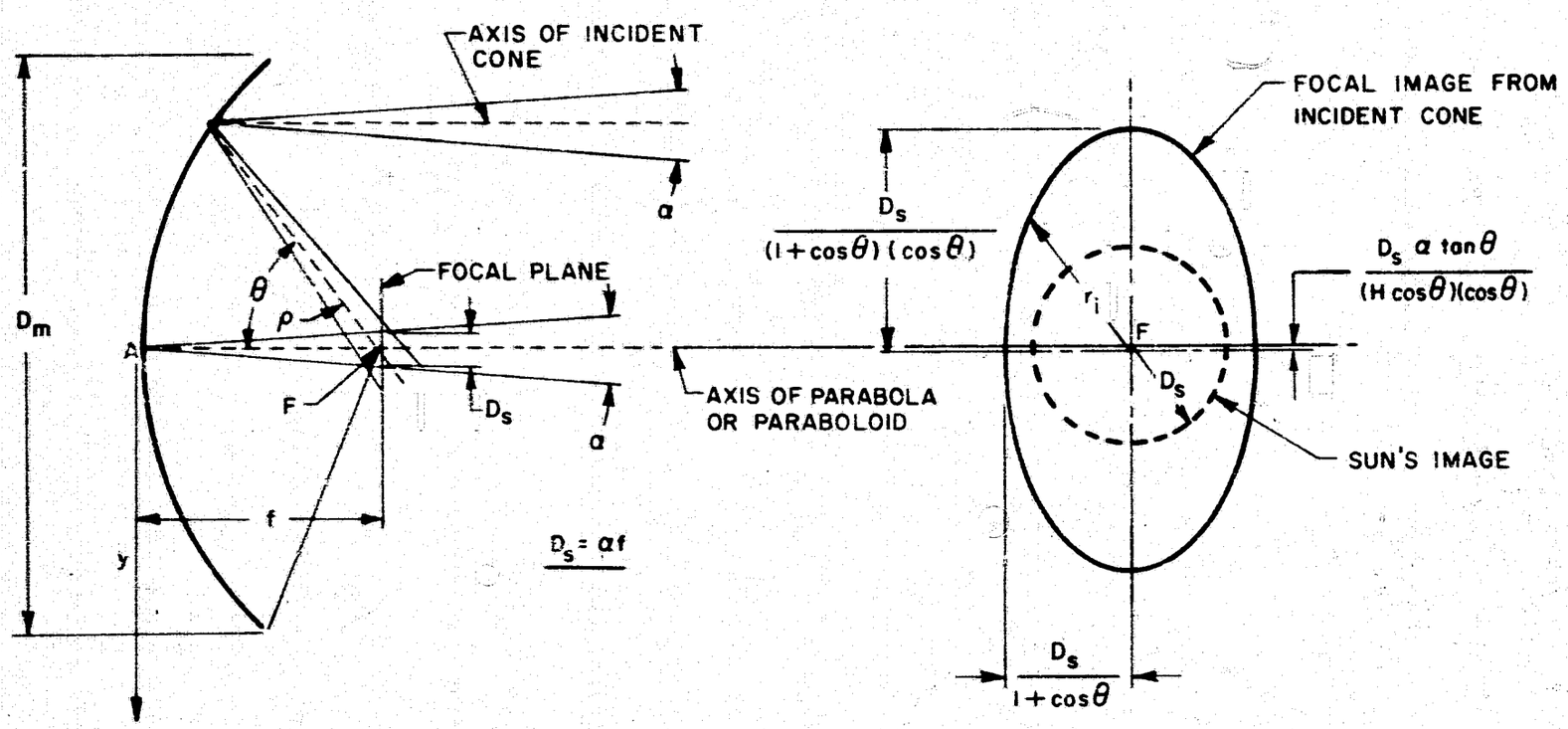

FIG. 3-9 PARABOLOID REFLECTOR CROSS-SECTION

4. Space environmental effects

5. Vehicle integration

   a. Volume and dimension limits

   b. Interference with other vehicle functions

It can be shown that the only type of absorber that will result in high efficiency at the temperatures of interest, is a cavity where the emitting-surface area is much smaller than the absorbing-surface area. This is demonstrated in Fig. 3-10 which shows the losses due to re-radiation and reflection from a black-body cavity and flat-plate absorber. Actual performance of flat-plate absorbers, based on presently available refractory materials, would be extremely poor, since absorptivity-emissivity values of less than 0.5 are normal for typical operating conditions. Another advantage of the cavity absorber is the design freedom afforded by its relative insensitivity to shape and size.

3.2.1 Collector-Absorber Efficiency

Analyses are available in the open literature that describe the performance obtainable from low-thrust systems as a function of thrusting time, exhaust velocity, powerplant specific weight, thrust, impulse, and other factors. These analyses have assumed that the powerplant specific weight is constant over the range of exhaust velocities of interest. This assumption is inaccurate in the case of solar propulsion.

The specific weight of the powerplant for the solar-hydrogen propulsion system, increases as the hydrogen-exhaust velocity increases, thereby effectively limiting the practical exhaust velocities (specific impulse) that can be achieved. This weight increase is due to the efficiency drop at high temperatures, as explained in the following simplified analysis.

The powerplant specific weight is defined as:

$$\begin{pmatrix}\text{powerplant}\\ \text{specific weight}\end{pmatrix} = \frac{\alpha}{\eta}\ (\text{lb/kw}) = \frac{\beta}{H\eta_i}\ (\text{lb/kw})$$

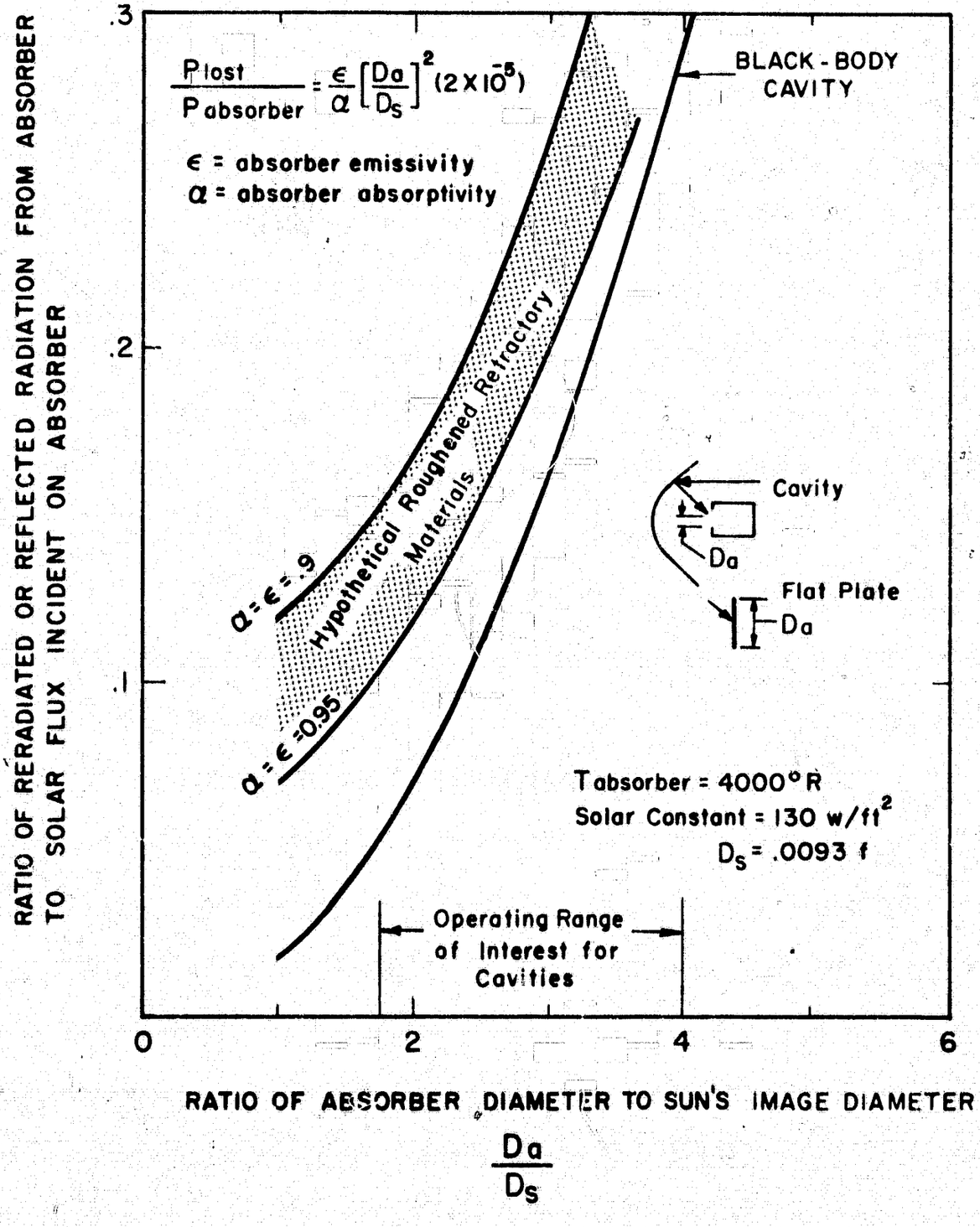

FIG. 3-10 RATIO OF REIRADIATED OR REFLECTED RADIATION FROM ABSORBER TO SOLAR FLUX INCIDENT ON ABSORBER VS RATIO OF ABSORBER DIAMETER TO SUN'S IMAGE DIAMETER

where

η = propulsion system efficiency

α = effective weight of powerplant per kw of solar power incident on system.

β = effective lb/ft^2 of concentrator (including structural supports)

H = solar flux kw/ft^2

Several efficiencies associated with the solar-hydrogen rocket thermionic power plant are shown in Fig. 3-11. These are:

1. Mirror efficiency - the amount of solar radiation that is reflected onto the useful area of the absorber, divided by the amount of sunlight falling on the system.
2. Mirror-absorber efficiency - the amount of energy kept by the absorber after re-radiation losses divided by the amount of sunlight on the system.
3. Propulsion System Efficiency - the power in the propellant flow divided by the sunlight on the system.
4. System Efficiency - The sum of the power in the propellant flow plus the electric power output divided by the amount of sunlight on the system.

For preliminary calculations, it is assumed that the absorber, located at the focal plane of the concentrator, is a cavity designed so that the maximum amount of sunlight will enter the cavity without an excessive amount of re-radiation from the entrance. It can be shown, that the use of a combined flat-plate and cavity-type absorber, will result in higher efficiency than obtainable with a single cavity absorber. This improvement is significant for poor quality mirrors, and only a few precent better for an ideal concentrator.

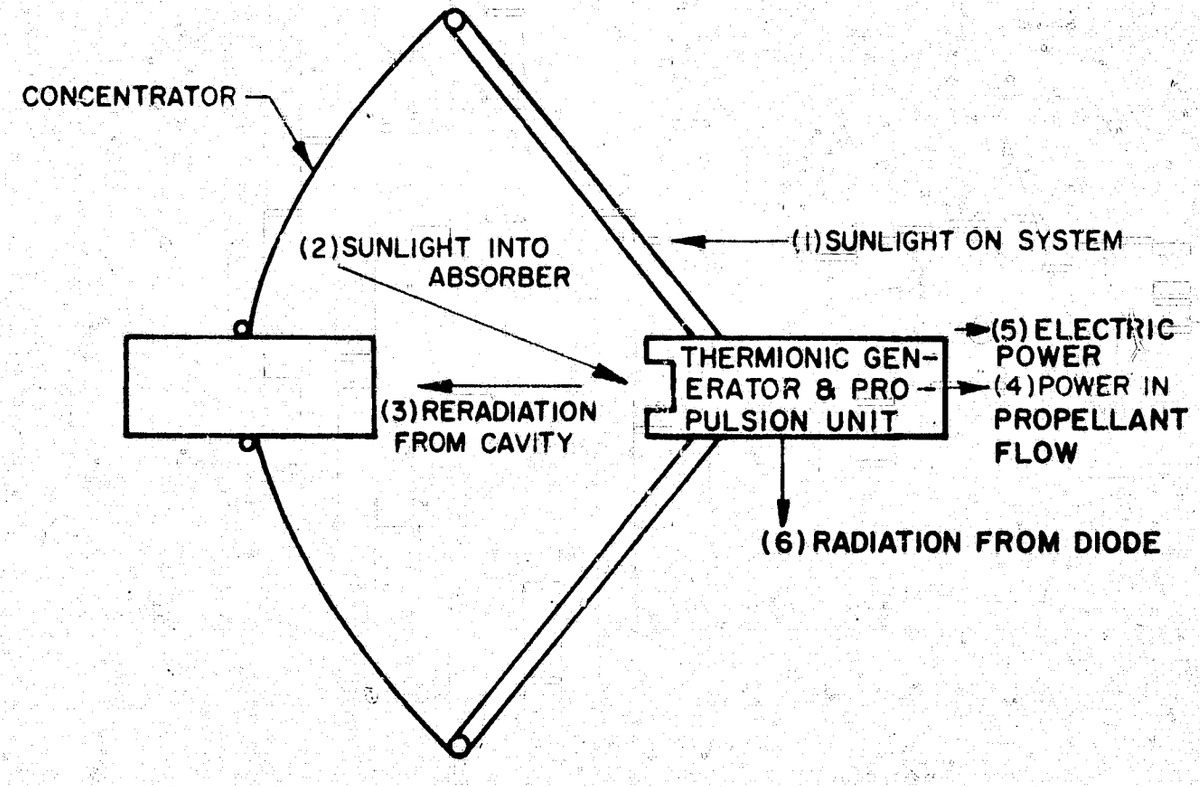

$$\text{MIRROR EFFICIENCY } \eta_m = \frac{(2)}{(1)}$$

$$\text{MIRROR-ABSORBER EFFICIENCY } \eta_{m-a} = \frac{(2)-(3)}{(1)}$$

$$\text{PROPULSION SYSTEM EFFICIENCY } \eta = \frac{(4)}{(1)}$$

$$\text{SYSTEM EFFICIENCY } \eta_s = \frac{(4)+(5)}{(1)}$$

FIG. 3-11 EFFICIENCY DEFINITIONS FOR SOHR-SET SYSTEM

Equations describing the heat balance of the absorber and mirror-absorber efficiency are given below.

$$HA_m\eta_m = A_{cav}\sigma T_{cav}^4 \epsilon_{cav} + GC_p(T_o - T_m) + Q_{lost} + Q_{nd}$$

$$\eta_{m-a} = \eta_m - \frac{A_{cav}\sigma T_{cav}^4 \epsilon_{cav} + Q_{lost}}{HA_m} - \frac{Q_{nd}}{HA_m} \qquad (3\text{-}1)$$

$$\eta_{m-a} = \eta_m - \frac{A_{cav}\sigma T_{cav}^4 \epsilon_{cav} + Q_{lost}}{H_o\left(\frac{1}{r}\right)^2 A_m} - \frac{Q_{nd}}{H_o\left(\frac{1}{r}\right)^2 A_m}$$

where

$Q_{nd} = P + Qrad$

$A_{cav}\sigma T_{cav}^4 \epsilon_{cav}$ = re-radiation from cavity

η_{m-a} = absorber-mirror efficiency

η_m = mirror efficiency

A_{cav} = entrance area of the cavity

σ = Stephan-Boltzmann constant

T_{cav} = effective cavity re-radiation temperature

ϵ_{cav} = effective emissivity of cavity

H = solar constant at r

H_o = solar constant = 130 w/ft^2 at 1 AU

r = distance from sun, AU

A_m = mirror area

P = electrical power output from diode

Q_{lost} = unavoidable heat losses due to radiation from support structures, etc.

Q_{rad} = thermal radiation from diode

G = mass-flow rate of propellant

C_p = heat capacity of propellant

T_0 = propellant outlet temperature

T_m = propellant cavity inlet temperature

The mirror efficiency associated with any given paraboloidal concentrator is a function of the ratio of cavity-entrance diameter to the sun's image diameter. For a concentrator with a perfect surface, all the sun's energy will be focused into a cavity-entrance diameter that is about $2.8D_s$ where D_s is the sun's image diameter at the focal plane defined by

$$D_s = 2 f \sin\left(\frac{\Theta}{2}\right) = \frac{.0093}{r} f$$

where

$\Theta = 32'$ at $r = 1$ AU

D_s = sun's image diameter

f = focal length of concentrator

The mirror efficiency, as a function of cavity-entrance diameter for a theoretically perfect concentrator, is shown in Fig. 3-12 for the specific case where the concentrator rim angle is 60° (near optimum value) and the surface reflectivity is 0.92. Also shown are a family of curves where mirror-absorber efficiency is plotted as a function of cavity-entrance diameter and the effective temperature of the cavity. The curves assume that Q_{lost} equals zero and the distance from the sun is 1 AU.

The optimum cavity-entrance diameter grows smaller as cavity temperature increases in order to compensate for re-radiation losses. As shown, η_{m-a} is a strong function of cavity temperature and consequently of the exhaust velocity of the hydrogen propellant.

It is possible to calculate the mirror efficiency, and from it the mirror-absorber efficiency, for any concentrator if a mathematical model is assumed that describes the deviations of the concentrator surface. Calculations at EOS have assumed that each cone of light reflected from the mirror crosses the focal plane at a distance from the focal point that can be described by a Gaussian distribution. This model is equivalent to a Gaussian distribution of the angular

η_{m-a} = MIRROR-ABSORBER EFFICIENCY

σ = STEFAN-BOLTZMANN CONSTANT

T_{cav} = EFFECTIVE TEMPERATURE OF RERADIATION

η_m = MIRROR EFFICIENCY

H = SOLAR CONSTANT = 130 W/ft^2

D_{cav} = CAVITY ENTRANCE DIAMETER

D_m = MIRROR DIAMETER

D_s = SUN'S IMAGE DIAMETER

f = CONCENTRATOR FOCAL LENGTH

$D_s = 0.0093\ f$

$$\eta_{m-a} = \eta_m - \frac{\sigma T_{cav}^4}{H_o}\left(\frac{D_{cav}}{D_m}\right)^2$$

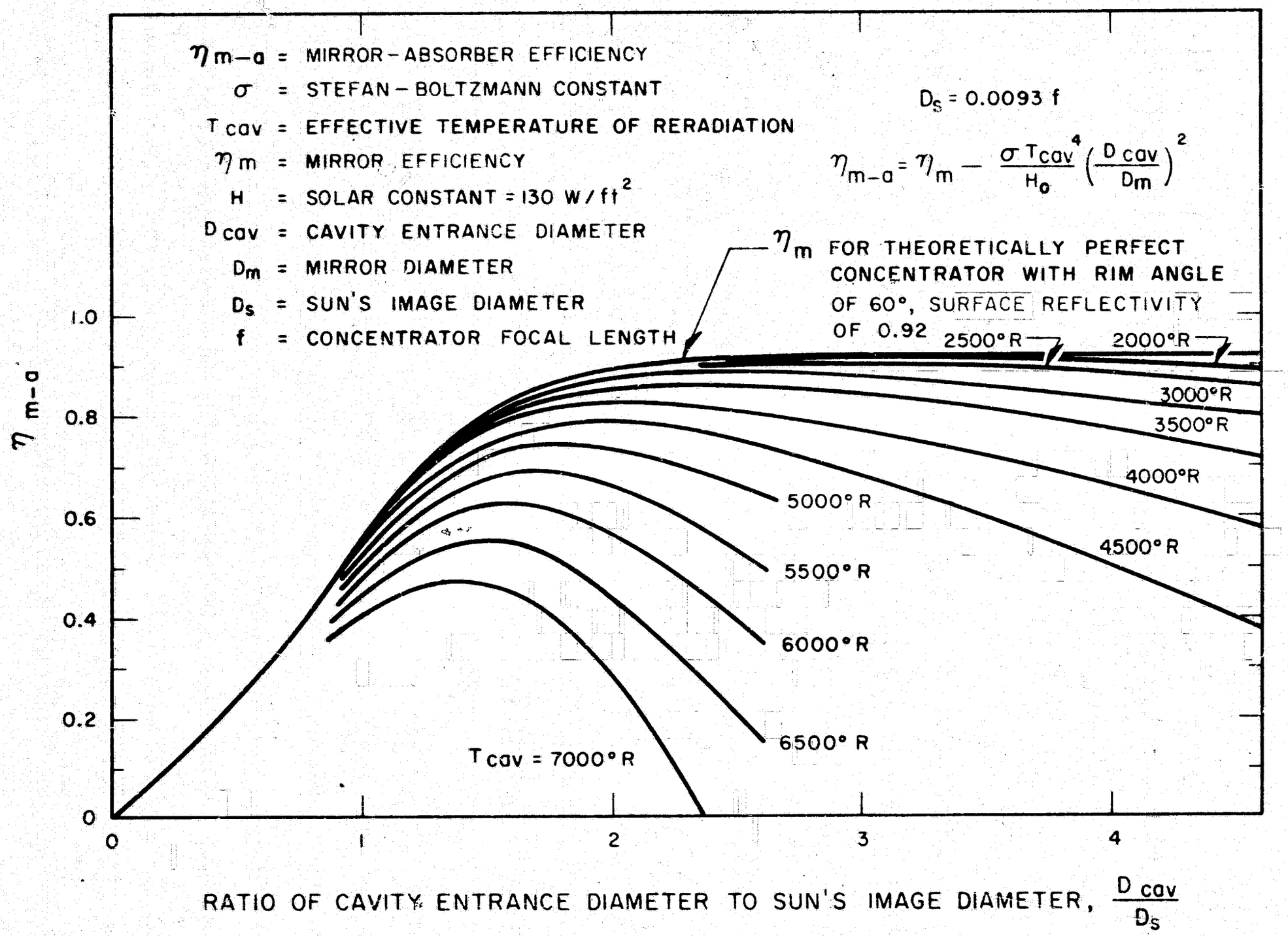

FIG. 3-12 MIRROR-ABSORBER EFFICIENCY VS RATIO OF CAVITY ENTRANCE TO SUN'S IMAGE DIAMETER AT 1 AU

deviations of the mirror surface. Note that for the case where T_{cav} is to be maintained constant then the optimum $\frac{D_{cav}}{D_s}$ will change as r changes. This is so because both D_s and H vary with r. Note also that η_{m-a} may either be calculated directly, or it may be found graphically (for ideal collectors) from Fig. 3-12. The method is as follows: First determine the value of $\frac{D_{cav}}{D_s}$ of interest, then find the value of η_{m-a} for r = 1, i.e., find η_{m-a} from Fig. 3-13. Subtract from the value the fraction of the total energy being used up by the diodes. The difference between η_{m-a} (Fig. 3-13) and the calculated value of η_{ma} is now multiplied by r^2 and the product subtracted from η_{m-a} (Fig. 3-13) to give the desired value.

The area between curves 2 and 3 of Fig. 3-13 represents the area of uncertainty for the future performance of 50 ft. diameter mirrors. Curve 3 is an estimate of the type of performance that could result by 1966 if development work continued in this area. Figure 3-13 also shows the maximum mirror-absorber efficiency for several paraboloidal concentrators as a function of cavity temperature. The curves are for a concentrator rim angle of 60°, and they show the effect of various types of surface degradation. Included in Fig. 3-13 is an estimate of the performance of 50 ft. collectors. Case 1 is for an ideal concentrator with no surface obscuration and a reflectivity equal to 0.92 (the maximum obtainable with aluminum). Cases 2 and 3 are the resultant curves for values of 0.5 and 0.25 degrees for the angular deviation. As shown, η_{m-a} drops to zero quite rapidly for high temperatures. Case 4 comes close to having a perfect surface geometry with a reflectivity of 0.88 instead of 0.92, and can be used as an indication of efficiency loss due to reflectivity loss.

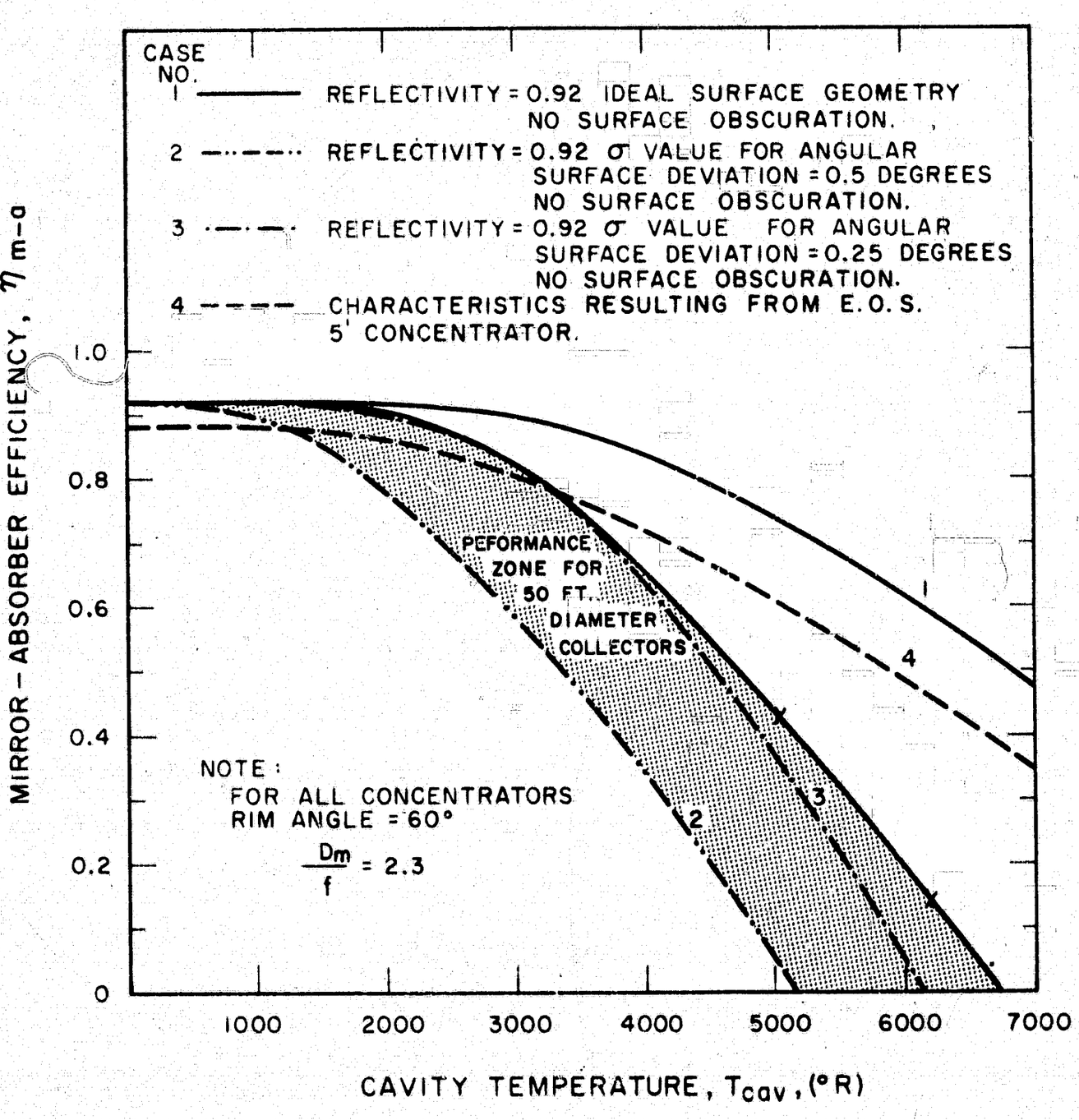

FIG. 3-13 MIRROR-ABSORBER EFFICIENCY VS CAVITY TEMPERATURE FOR VARIOUS LEVELS OF ANGULAR SURFACE DEVIATION

The effect of misorientation on collector-absorber efficiency becomes more serious at the higher cavity temperatures. A limit of about 30 min. of angular error is required to achieve acceptable efficiencies at cavity temperatures above 2000°K. The maximum rim angle, before performance becomes seriously degraded, is about 60°.

Specific weights of solar collectors at present appear to be about 0.5 lbs per sq. ft. for units ranging from 5 feet to 40 feet in diameter. Figure 3-14 gives the weights of representative collectors as a function of diameter. Even though the rigid collector is the heaviest of them all, due to the accuracy inherent in its fabrication, it is able to deliver more energy at a higher temperature on a per unit weight basis than any of the other systems. It is likely that improved techniques and advanced materials may decrease the specific weight by a factor of two in the near future, if continued emphasis is placed on this area of development. It appears reasonable to anticipate that values of α in the range of 2-4 lbs. per kw will be achieved for relatively high performance space mirrors. The curves for the maximum thrust and the maximum power available at 1 AU are shown in Figs 3-15, 16 respectively. To find the value of thrust and electric power at other distances from the sun, one need only find the efficiency at the given point in space by equation (3-1), or by the graphical method outlined previously. The new value of thrust or electrical power output is the product of this new value of efficiency and the thrust or electrical power output, whichever is applicable, divided by the value of the efficiency, at one Astronomical Unit.

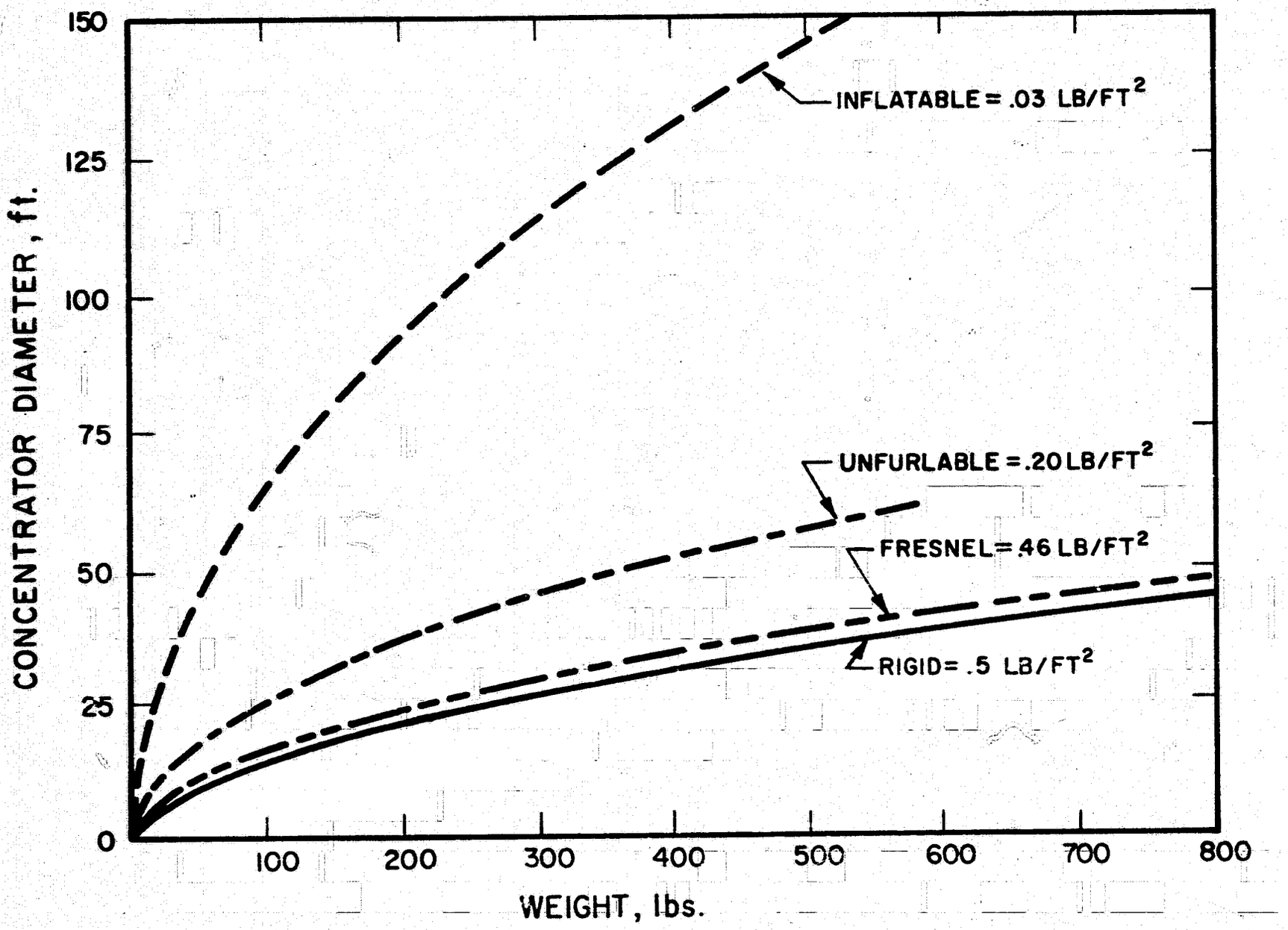

FIG. 3-14 CONCENTRATOR DIAMETER VS WEIGHT

Corrected October 1962

$$P_{kw} = \frac{F\ I_{sp}}{45.8\ \eta_{m-a}\ \eta_n}$$

η_{m-a} = mirror-absorber efficiency

η_n = nozzle energy efficiency = 0.85

H = solar flux = 130 watts/ft^2

I_{sp} = 800 sec.

700 sec.

600 sec.

D - CONCENTRATOR DIAMETER (FT.)

F - THRUST (LBS)

FIG 3-13 MIRROR DIAMETER VS THRUST AT 1 AU

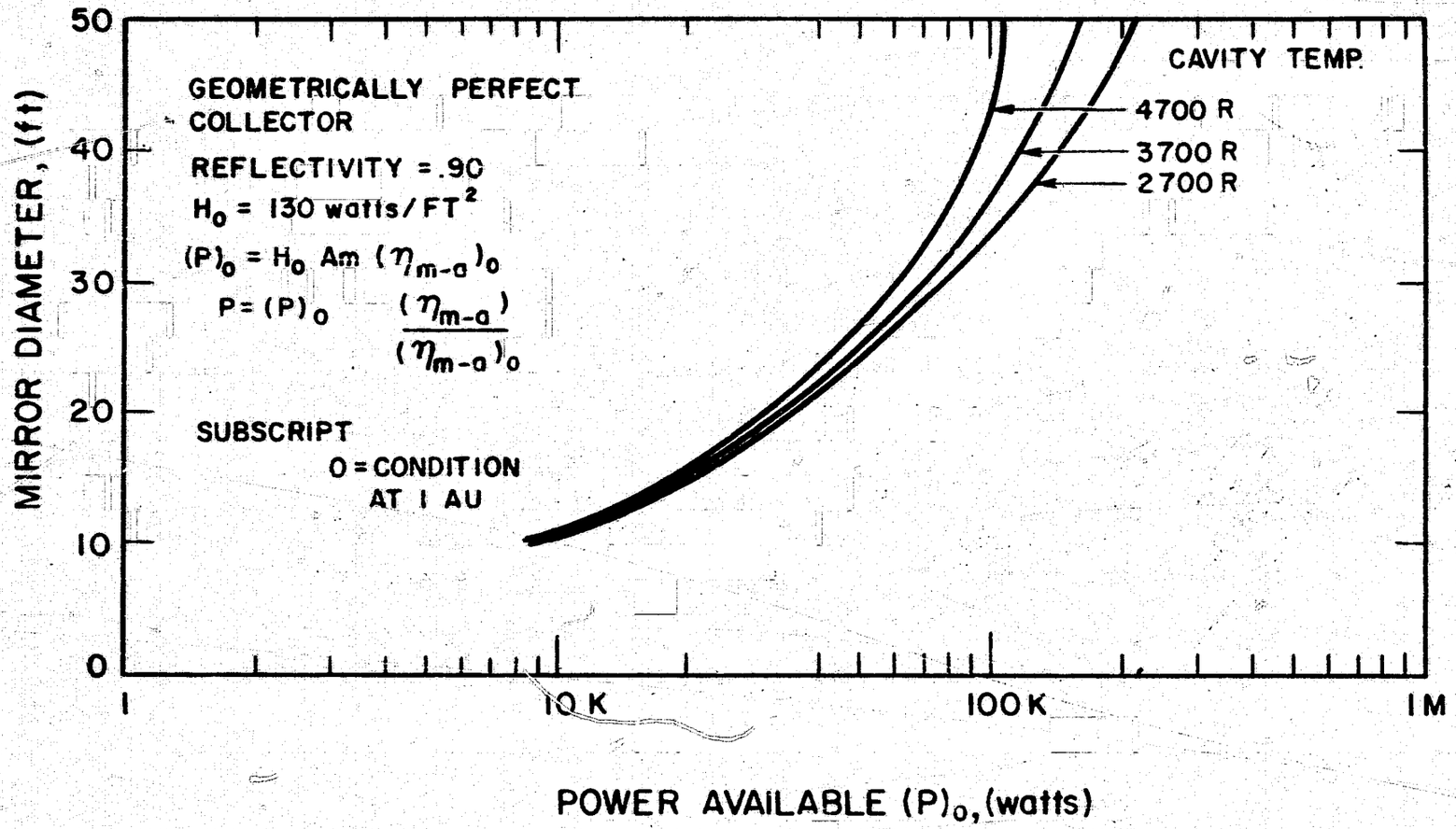

FIG. 3-16 MIRROR DIAMETER VS POWER AVAILABLE AT 1 AU

3.3 Diode Characteristics

3.3.1 Thermionic diodes operate on the principle wherein hot surfaces emit electrons according to Richardson's equation. When surfaces at different temperatures, and emitting electrons at different rates are connected through an external circuit, then an electric current will flow. The first step towards getting useful amounts of electric power out of such a device is to try to eliminate the space charge which tends to develop between an anode and a cathode of such a device. The most accepted method used at the present time is a source of positive ions (cesium) introduced in the interelectrode gap and used to neutralize the excess electrons forming the space charge. In conditions where the space charge is assumed to be negligible, the diode efficiency is given by

$$\eta_D = \frac{(\phi_C - \phi_A) J_{ext}}{J_{ext} (\phi_C + 2 k T_C) + Q_{str} + Q_r + Q_{cesium}}$$

J_C, J_A, = cathode and anode current respectively as given by Richardson's equation

J_{ext} = external current

ϕ_C, ϕ_A = cathode and anode work functions respectively

k = Boltzman constant

Q_{cesium} = heat conducted away from cathode to anode by cesium vapor.

Q_r = heat lost by radiation from cathode to anode.

Q_{str} = heat conducted away from cathode by support structures.

T_C = absolute temperature of cathode face

The output voltage is proportional to $\phi_C - \phi_A$. To have a highly efficient thermionic diode $\phi_C - \phi_A$ should be made as large as possible, J_A should be a small fraction of J_C, Q_{cesium} and Q, should all be made as small as possible. In the design of a diode care has to be taken to exclude any foreign gases that may tend to upset the neutralizing effect of the cesium ions. The design must also be such that the proper spacing results at the operating temperature. The cathode and anode materials must also be such that they have low vapor pressures and so prevent a build up of one on the other. During operation the electrodes must not undergo changes in crystal orientation or growth that may adversely effect the diode performance.

Figure 3-17 is a plot of thermionic diode performance versus emitter temperature. Although a diode efficiency of 20 percent is indicated at 3400°F, such a system cannot presently be built to operate over any prolonged period of time due to materials limitations, and systems for missions contemplated in this report are expected to have an efficiency of approximately 10-15 percent at emitter temperatures of about 3100°F.

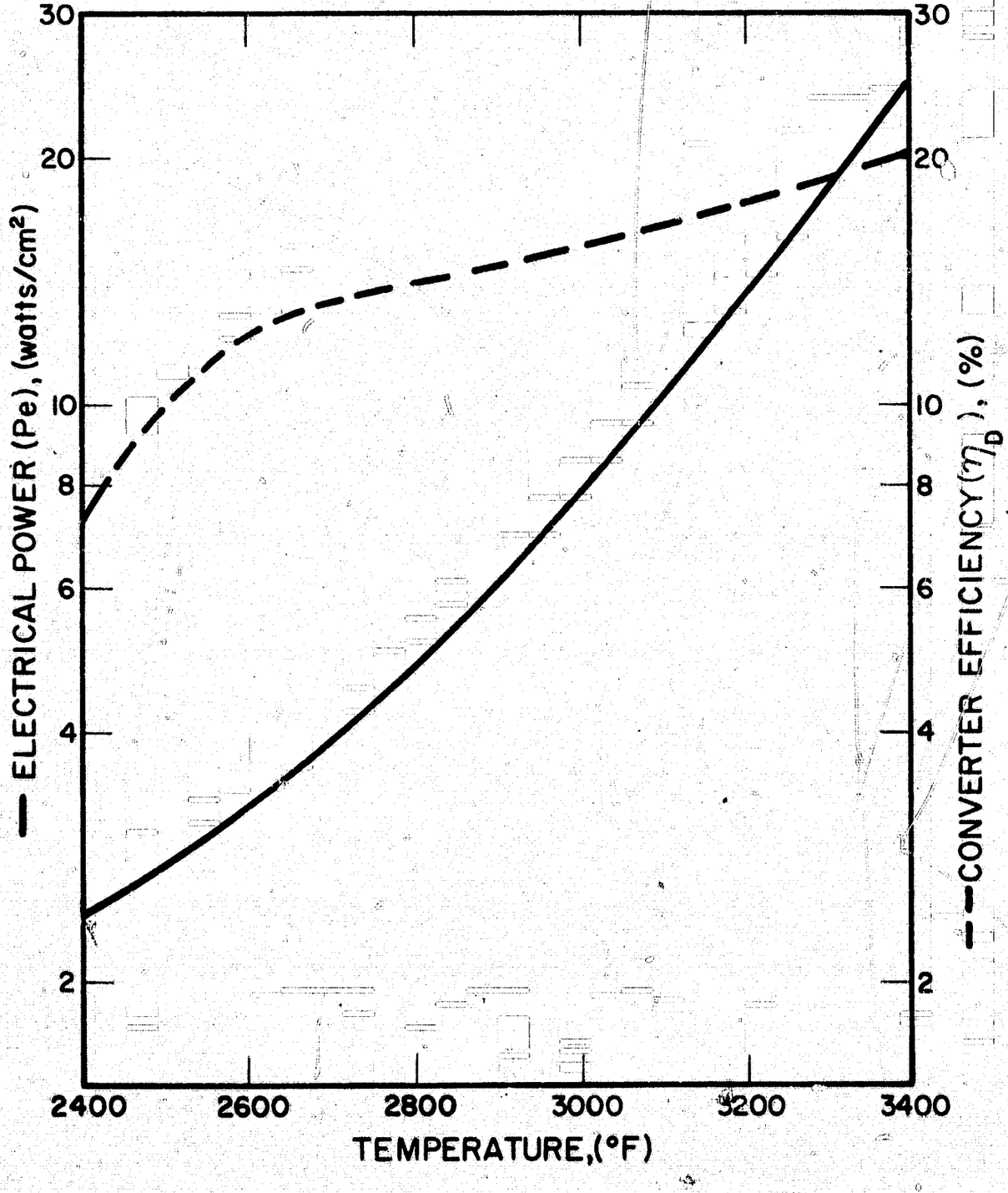

FIG. 3-17 THERMIONIC DIODE PERFORMANCE VS EMITTER TEMPERATURE

3.4 Thermal Energy Storage

Due to the high operating temperature of the SOHR-SET system thermal cycling must be eliminated in order to prevent the reduced operational life which is a consequence of such cycling. Cycling will occur if the space craft passes through the shadow of the earth or other planet, or if there is a momentary misorientation of the solar collector. If thermal energy is stored in the cavity, cycling can be damped out by this heat reservoir.

There are three basic requirements for thermal energy storage (TES) devices.

1. High thermal capacity in terms of energy stored per unit weight and volume.
2. The capability of many charge and discharge cycles without degradation.
3. Isothermal discharge temperature.

Among the possible methods of TES are heat storage by thermal capacity, order-disorder transitions, heat of fusion, heat of vaporization, thermochemical reaction, heat of sublimation. Most investigators have concluded that TES using heat of fusion is a technique worth developing (Ref. 3, 4) and nearly all of the development work is in this area. Furthermore heat of fusion TES is the only method sufficiently developed for consideration regarding application to the 2,200-2300°C temperature range of interest for the SOHR-SET system.

Most TES research and development work has been geared to the 800-2200°K range. However, the knowledge gained here is applicable to higher temperatures. Empirical relationships have been developed for the estimation of heat of fusion and there are known materials with melting points in the range of interest, but the problem is more complex. Handling and preparation problems are

usually the overwhelming ones since mixtures of MgO, BeO, CaO, Al_2O_3 can usually be tailor made for fusion in the temperature range of interest. These TES materials can be expected to yield heats of fusion greater than 100 and less than 250 watt-hrs/lb.

TES material will either be placed in the wall of the cavity or sealed in containers which will be located in the cavity. Significant progress is being made in the thermal-design and fabrication problems associated with TES material containment. The literature will be checked further, with the continued aim of getting particular information on TES material and technology for the very high temperature range.

4. DESIGN STUDY OF COMBINED CAVITY ABSORBER

4.1 Introduction

There are four important subsystems in the design of a combined cavity absorber.

1. The cavity entrance flux control and top plate
2. The hydrogen heat transfer coils
3. The diodes
4. The thermal energy storage system

4.2 Cavity Entrance, Flux Control, and Top Plate Considerations

The top plate is designed as a flat plate absorber so that any stray incoming radiation can be utilized as a pre-heat system for the gas entering the cavity. In this respect, top plate design criteria are in no way different from that for a SOHR. With regards to flux control, the answer is that a rather versatile flux flap is required. During the period of time that the cavity is receiving energy from the sun, the ratio of the cavity diameter to the sun's image diameter must be maintained constant for optimum absorber efficiency. If the spacecraft distance from the sun is constantly changing, then the flux flaps must be capable of adjusting the cavity diameter or the effective cavity diameter, accordingly since the sun's image diameter will vary inversely as the distance from the sun over the range of distances of interest to us. During the period of time when the SOHR- SET is receiving its energy from its heat reservoir, energy then the ideal condition is to have the cavity opening closed. Hence, not only must the system be capable of modulating solar influx to the cavity, but it must be capable of literally closing off the cavity entrance during nighttime to conserve the thermal energy storage. For a spacecraft operating between 0.3 and 2 AU this translates into a

requirement that the flux flaps be capable of closing off the cavity completely, and also be capable of vernier type operation between the 15 percent opening to the fully open position. It is conceivable to design such a flap by having the cavity temperature operate the vernier-like positioning mechanism, and by having the presence or absence of stray flux on the top plate operate a normally closed device. Current design practice is to have the cavity diameter approximately 1 percent of the collector diameter at 1 AU.

4.3 Design Considerations for the Hydrogen Heat Transfer Coils

In the cavity, the hydrogen is heated by passing it through molybdenum, rhenium, or molybdenum-rhenium coils which are heated by the isothermal cavity conditions, and by the direct impingement of the incoming solar radiation. The coils must be arranged in the cavity in such a fashion that the hottest point occurs at the point of exit of the gas stream. In order to do this the geometric configuration of the coil becomes very important since this determines the intensity of the incident solar radiation. The incident solar radiation is given by

$$Q_s = \frac{4f^2 H \eta_m}{R_o^2} \quad \frac{\sin^3 (\alpha + \theta)}{\cos^2 \alpha \, (1 + \cos \theta)^2}$$

where

Q_s = incident solar radiation per unit area

f = focal length of collector

R_o = radius vector from focal point to point under consideration

α = half angle of conical surface on which coils lie ($\alpha = 0$ for cylindrical cavity)

θ = angle between cavity axis and line from focal point to point under consideration

The value of α is usually chosen as 30 degrees to minimize the coil length, the maximum flux on a 30 degree coil is given by

$$Q_{s_{max_{30}}} = \frac{0.445 \quad 4f^2 H \eta_m}{R_o^2} \qquad (4\text{-}1)$$

For a coil design utilized as per Fig. 4-1, the intensity of the incident solar radiation decreases as the distance from the focal plane increases. From a heat balance about the element of the exit section of the heating coil receiving the most intense solar radiation, it can be shown that

$$Q_H \approx \alpha_s Q_s \approx h (T_{we} - T_b)$$

where

Q_H = energy transferred to hydrogen
α_s = absorptivity at solar wavelengths
h = heat transfer coefficient
T_{we} = wall temperature at exit
T_{be} = hydrogen bulk temperature at outlet, $4000^{\circ}R$

If

$$T_{we} - T_{be} = 400$$

$$Q_s \approx \frac{400}{\alpha_s} h$$

For laminar flow (and this is usually the case)

$$H = \left(\frac{k_H}{d_t} \right) \left[5.14 - (0.78) (T_{we}/T_{be}) \right]$$

where d_t = tube internal diameter
k_H = thermal conductivity of hydrogen at $4000^{\circ}R$
$\approx .58$

hence maximum allowable value of Q_s is

$$Q_{s_{max}} = \left(\frac{400\ k_H}{\alpha_s\ d_t} \right) \left[5.14 - (0.78)(T_{we}/T_{be}) \right]$$

where $Q_{s_{max}}$ is given by equation 4-1.

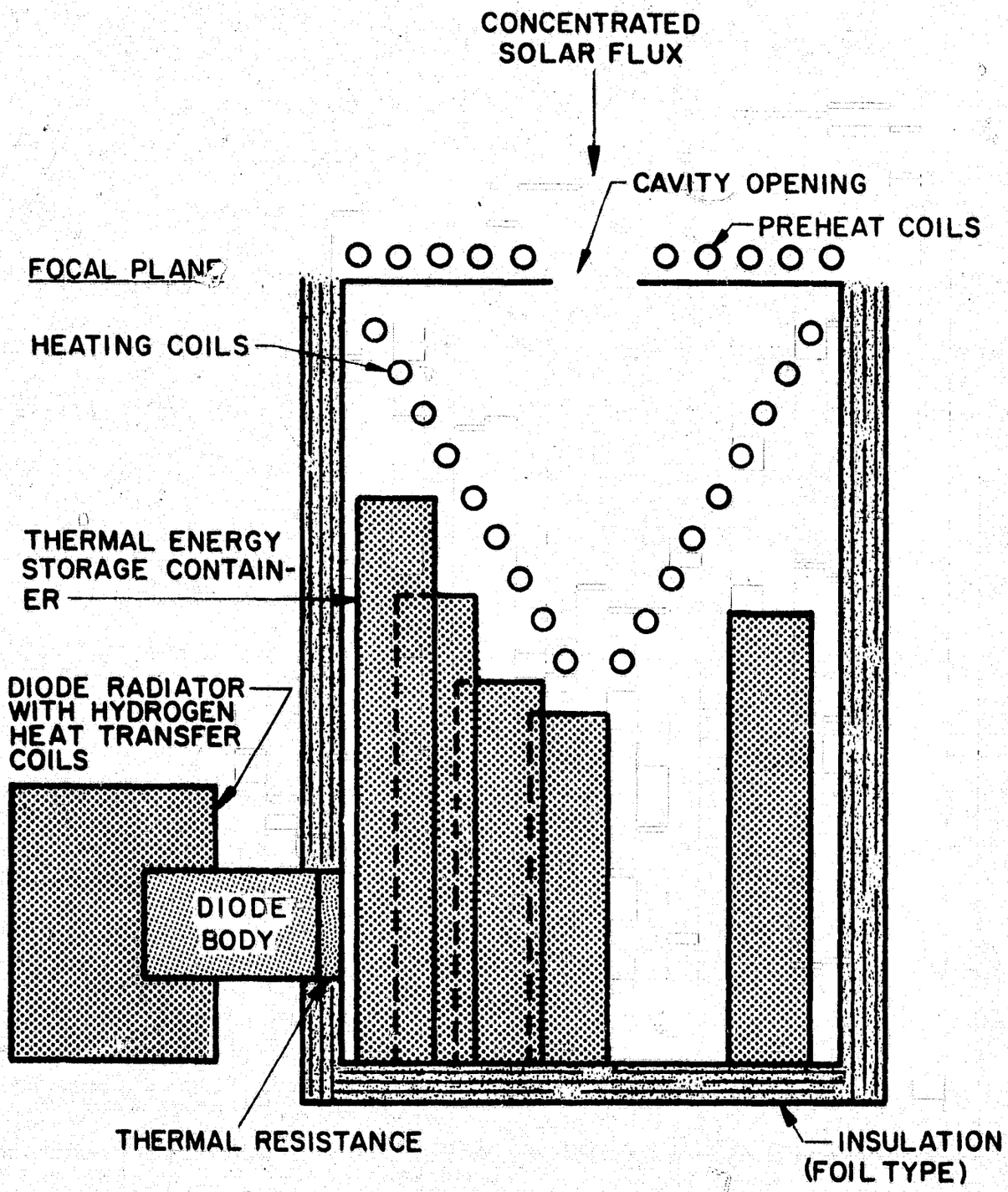

FIG. 4-1 INTEGRAL SOHR-SET CAVITY DESIGN CONCEPT

Design considerations leave no choice as to coil placement. The coil must be placed in the foremost position of the cavity with the base of the cone closest to the focal plane and with hydrogen entering near the apex.

4.4 Integration of the Thermionic Diodes

Two major considerations dictate the manner by which the thermionic diode is incorporated in a combined cavity absorber. One consideration is the fact that the thermionic diode emitter face operates at a temperature approximately 1,000°F less than the optimum for the SOHR aspect of the design; hence, some manner must be found to deliver heat to the emitter face of the thermionic diode at a lower temperature. The second consideration is coupled with the first and is the requirement that the temperature on the emitter face must be uniform. These considerations rule out placing the diodes in the forward part of the cavity; here the direct solar radiation is most intense and the variation steepest. The diodes must be placed in the rear of the cavity preferably in the shadow of the coils and the thermal energy storage containers (Fig. 4-1).

To transfer the heat to the emitter face at a 1,000°R temperature difference three general approaches have been considered. Two of these approaches are shown in Fig. 4-2. These two approaches can be used in conjunction with the conventional type diode configuration in which both the emitter and the collector are flat discs. The third temperature reduction mode is via radiative transfer to a secondary cavity in which the diode is located.

If the secondary cavity is a long slender cylinder with a diameter of approximately 1 inch, it then becomes feasible to use one large diode rather than a set of diodes as must be the case in the first two design concepts. Even though a single large diode may not be desirable from the standpoint of overall electrical system reliability, the ability to make large diodes is desirable for high-powered electrical systems.

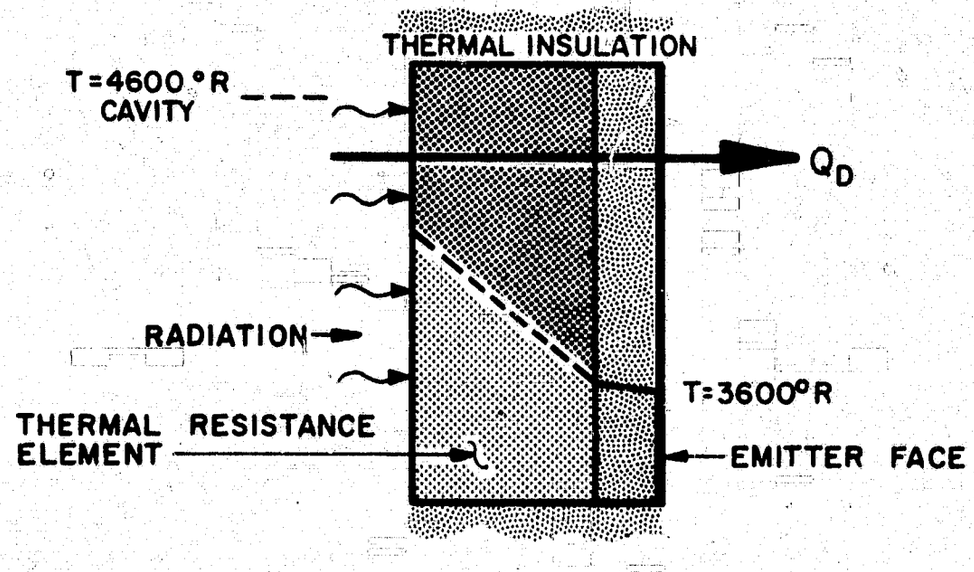

(A) TEMPERATURE RESISTANCE ELEMENT

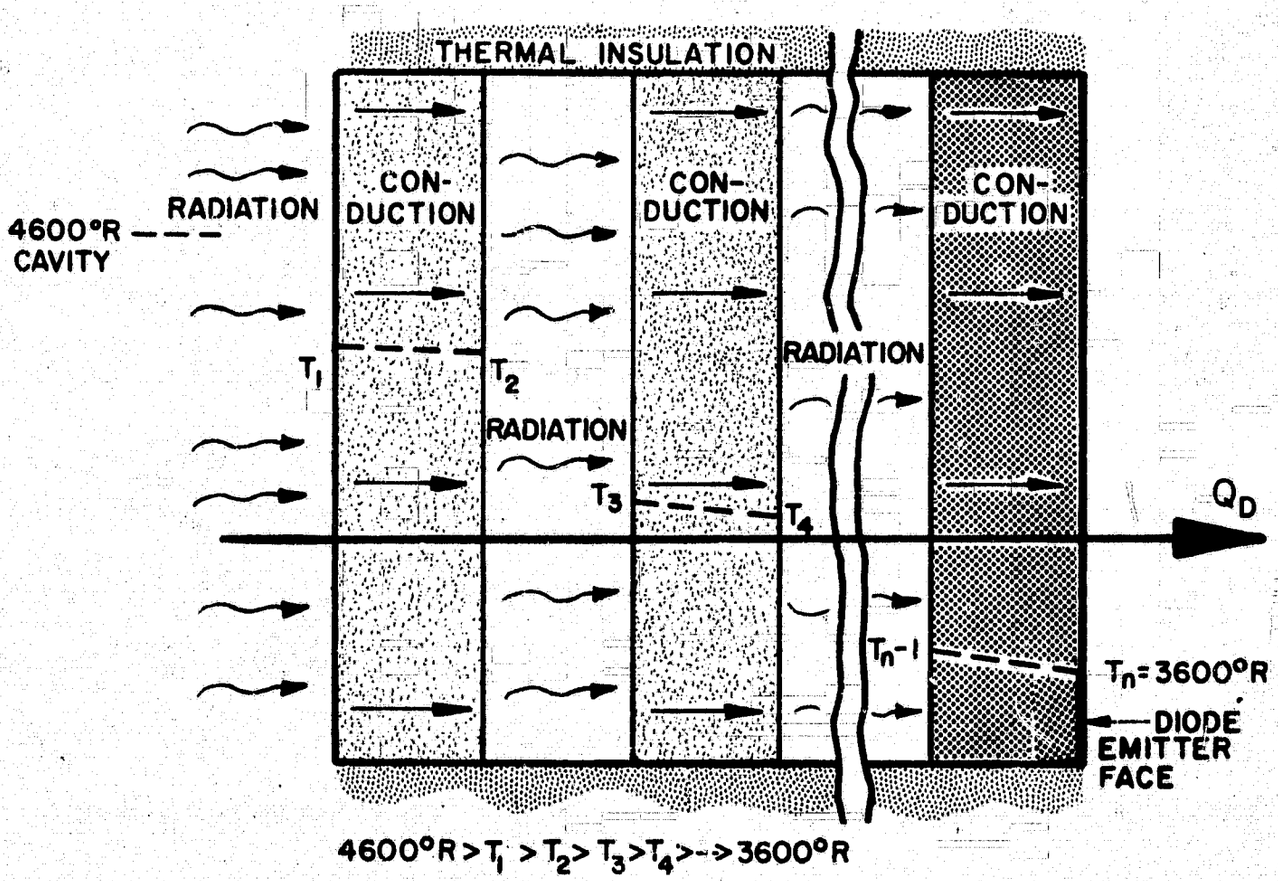

$4600°R > T_1 > T_2 > T_3 > T_4 > \cdots > 3600°R$

(B) TEMPERATURE REDUCTION BY RADIATION AND RESISTANCE ELEMENTS IN SERIES

FIG. 4-2 MODES OF HEAT TRANSFER FROM CAVITY TO DIODE EMITTER

In Fig. 4-2A, the heat is first transferred by radiation from the cavity to the surface of the thermal resistance element, then conducted with the required temperature drop to the diode emitter element. The required emitter drop across the resistance element may be large or small depending upon the fraction of the temperature drop which occurs as a consequence of the radiative heat transfer to the surface of the thermal resistance element. The temperature drop due to radiative heat transfer will be large if the emissivity of the thermal resistance element is small, and small if the converse is the case. If the emissivity of the thermal resistance element is equal to 0.9, then substantially all of the temperature drop must occur across the thermal resistance. Whereas, if the emissivity is equal to 0.3, then substantially all the temperature drop occurs as a consequence of radiation from the cavity to the surface of the resistance element. The derivation of the equations from which these conclusions were drawn are shown below. From a heat balance about the wall face of the resistance element

$$T_w = \left(T_c^4 - \frac{Q_D - \alpha_s Q_s}{\sigma \epsilon} \right)^{1/4}$$

T_w = absolute wall temperature of thermal resistance element

T_c = absolute cavity temperature

T_e = absolute temperature of emitter face

Q_D = diode heat flux

Q_s = incident solar radiation

α_s = absorbtivity at solar wavelengths

σ = Stefan-Boltzmann constant

ϵ = emissivity of wall of thermal resistance element

for $Q_s = 0$

$$T_w = \left(T_c^4 - \frac{Q_D}{\sigma \epsilon} \right)^{1/4}$$

now

$$Q_D = \frac{\Delta T}{X} \left[\frac{1}{\underbrace{\left(\frac{1}{k}\right)}_{\text{resistance element}} + \underbrace{\left(\frac{1}{k}\right)}_{\text{emitter}}} \right]$$

$$= \frac{km}{X} \Delta T$$

where k = thermal conductivity

ΔT = temperature drop

X = length of heat transfer path

hence $$T_w^4 + \frac{k_m}{X \sigma \epsilon} T_w - \left(T_c^4 + \frac{k_m T_e}{X \sigma \epsilon} \right) = 0$$

In practice $Q_o = \frac{\text{diode output per unit area}}{\text{diode efficiency}}$

This data is given in Fig. 3-17 as a function of emitter temperature

Figure 4-2B illustrates the use of the radiation and conduction modes of heat transfer in series. With this type of arrangement it is possible to have almost all of the temperature drop occur as a consequence of radiation heat transfer and hence, reduce the distortion of the temperature field. If adequate control can be achieved over the emissivities of the radiating surfaces, significant temperature reductions can be achieved in a single step. For example, for a high temperature face at 4,600°R and an emissivity equal to 0.3, transferring heat to a lower temperature face with emissivity equal to 0.9, the low temperature face equilibrates at a temperature below 3,500°R. The exact temperature depends upon the amount of heat being transferred. Hence, it appears feasible that the diode will be able to function simply by radiative heat transfer from the cavity wall to the emitter element, provided that the emissivity values can be maintained constant throughout the desired diode lifetime. The relationship between the high and the low temperature surfaces is given by

$$T_{i+1} = \left(\frac{1}{\epsilon_{i+1}} \right)^{1/4} \left(\epsilon_i T_i^4 - \frac{Q_{i+1}}{\sigma} \right)^{1/4}$$

where the subscript i tags the higher surface temperature.

In order to regenerate a fraction of the heat rejected by the diode collector, the diode heat rejection system must be designed so that during thrusting, all the heat that can be transferred is transferred to the incoming hydrogen, and the unavailable remainder rejected by the diode radiator. Figure 4-3 is a design concept for such a system. The degassing and scavenger chambers shown are necessary to prevent the hydrogen diffusion from the coils to the diode. In the degassing chambers the hydrogen and the metal diffuses out into the near vacuum maintained by the scavenger chamber. The scavenger chamber maintains the near vacuum by reacting with any free hydrogen to form a compound which has a very low equilibrium hydrogen pressure at the temperature at which it is maintained. It should be noted that at times it may be best to make the radiator flat rather than cylindrical.

The quantity of heat recovered from the thermionic system is given by

$$Q_{reg} = 1.055\ \dot{\omega}\ \bar{C}_p \Delta T_H \quad \text{Kwatts}$$

$\dot{\omega}$ = hydrogen flow rate to cavity, pounds /sec

$\bar{C}_p$ = mean specific heat of hydrogen over temperature range of interest

= 3.5 BTU/pound

Q_{reg} = regenerated diode heat

remembering that

$$P = \eta_D Q_D$$

it follows that

$$Q_{\eta D} = P + Q_{rad} = Q_D - 1.055\ \dot{\omega}\ \bar{C}_p\ \Delta T_H$$

Since the hydrogen enters at approximately 50°K and the collector temperature is approximately 1000°K, then allowing for a 25°K temperature difference for both ends of the heat transfer device, the maximum

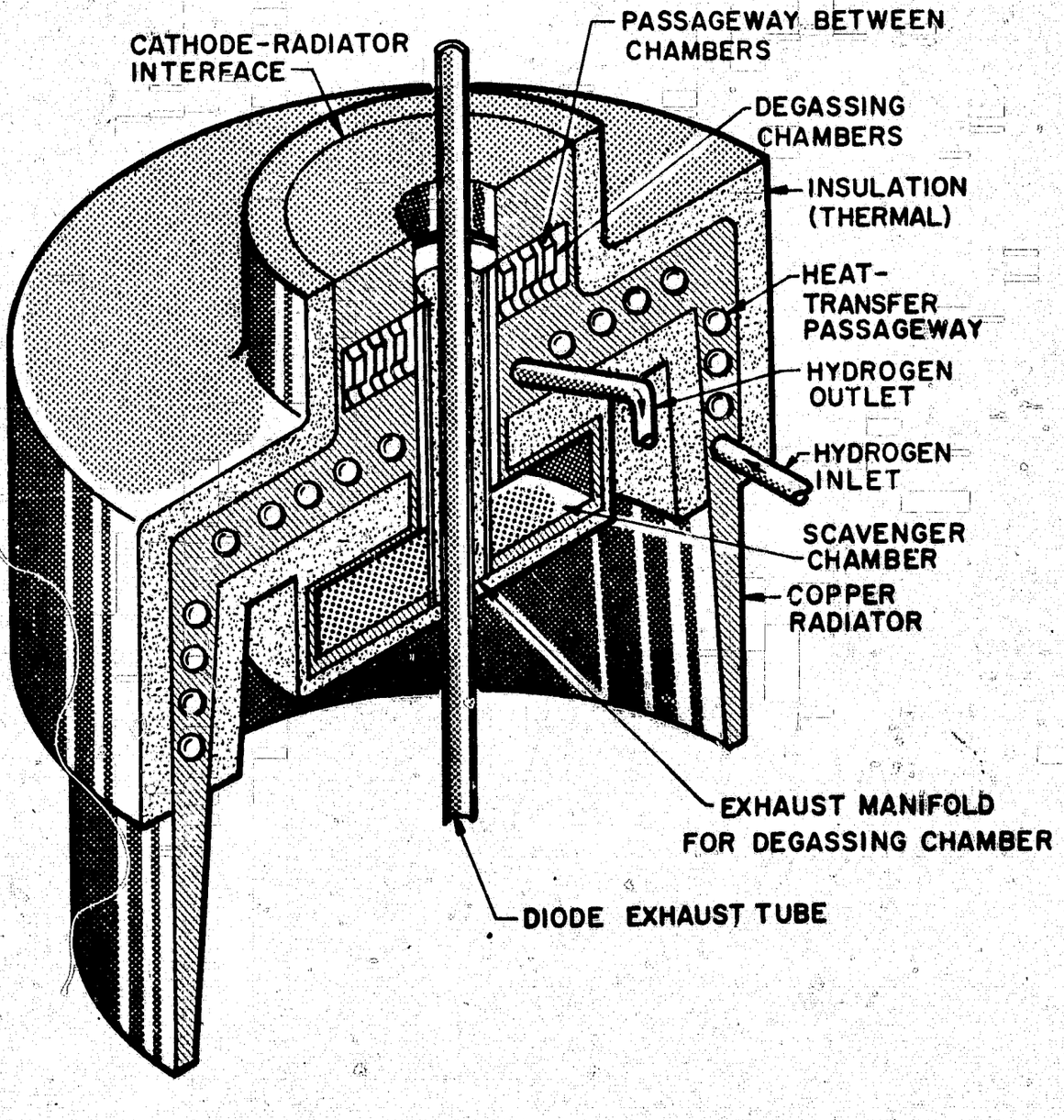

FIG. 4-3 INTEGRAL REGENERATIVE AND RADIATION COOLED DIODE HEAT REJECTION SYSTEM

practical ΔT_H seems to be 1530°F. This yields

$$Q_{reg} = 5.65 \times 10^6 \dot{\omega} \text{ watts}$$

From equation 3-1

$$\eta_{m-a} = \eta_m - r^2 \left[\frac{A_{cav} \sigma T_{cav}^4 \epsilon_{cav} + Q_{post} - Q_D + 5.65 \times 10^6 \dot{\omega}}{H_o A_m} \right]$$

The ratio

$$\frac{5.65 \times 10^6 \dot{\omega} r^2}{H_o A_m}$$

is the increase in the mirror-absorber efficiency due to regeneration. The ratio

$$\frac{5.65 \times 10^6 \dot{\omega}}{(P/\eta_D)}$$

is the fraction of thermionic system heat flow that is regenerated and the maximum possible regeneration occurs when

$$\frac{5.65 \times 10^6 \dot{\omega}}{P/\eta_D} = 1 - \eta_D$$

Stated otherwise, when

$$P < \frac{5.65 \times 10^6 \dot{\omega}}{(\frac{1}{\eta_D} - 1)}$$

All the diode waste heat is being returned to the cavity. For a SOHR-SET system with $\eta_D = 0.15$ and $I_{sp} = 800$ sec., P must be less than 1,125 X F(where F is the thrust level in pounds) in order to have 100 percent regeneration of diode waste heat.

4.5 The Thermal Energy Storage System

The thermal energy storage system can be placed either in the walls of the cavity or in the body of the cavity. It is preferable to place the thermal energy storage system in the rear of the cavity and make the cavity longer rather than wider. This is done in order to keep the projected area of the cavity small and hence, the mirror efficiency high. An important function of the thermal energy storage containers is to shield the diode locations from direct solar radiation.

4.6 The Hydrogen Diffusion Problem

The picture is not clear regarding the magnitude of the effect of hydrogen on the functioning of diodes, nor is it clear just how much hydrogen may be expected to diffuse into and be absorbed by the diode. There are, however, some general statements that may be made regarding the problem.

Tantalum, niobium, and titanium are metals which are used in diode construction. These metal parts may become embrittled if they operate in atmospheres of hydrogen 10^{-5} to 10^{-4} mm of mercury for any prolonged periods. In the 300-500°C temperature range, they become so brittle that they crumble into a powdered mass. Above 500°C, their behaviour is peculiar in that they out-gas in a manner not clearly understood.

In the 10^{-4} to 10^{-3} mm pressure range, the diode emitter and collector surfaces may become affected. In the 1 mm pressure range, diode operation is affected if the total electron cross section area of hydrogen approaches the total electron cross section area of cesium. Thus, care must be taken to isolate the diode bodies to prevent the hydrogen pressure from exceeding a pressure which is between 10^{-5} to 10^{-3} mm of mercury.

Hydrogen diffusing into the cavity will be in equilibrium with the hydrogen leaving the cavity entrance and going into the space vacuum. It is quite possible that the equilibrium cavity hydrogen pressure will be very small and attempts will be made to estimate this.

A desirable situation would be for the equilibrium pressure to be less than 10^{-5} mm of mercury.

Very little data is available for the diffusivity of hydrogen through molybdenum. None appears to be available for diffusion of hydrogen through molybdenum-rhenium alloys. Attempts will be made to estimate these diffusivity values at the high temperature of the coil walls. The effect of hydrogen on diodes is currently being studied by the Radio Corporation of America on a Government contract, and the results of this study should be invaluable if the hydrogen diffusion problem proves to be a difficulty.

5. MISSION STUDIES

5.1 Introduction

Due to its simplicity of design, presumed high reliability and reasonably high specific impulse (600-800 sec.), the SOHR-SET concept appears ideally suited to the task of providing continuous thrust and electrical power for near-sun space missions. A space mission of particular interest is that in which a probe is sent to within approximately 0.3 Astronomical Units from the center of the sun in order to obtain data regarding the atmosphere and surface of the solar body. In order to justify the use of a SOHR-SET for this type of mission, its performance must be compared with that of current, or foreseeable, propulsion devices. Only two such devices are considered here, namely, the ordinary chemical rocket and the ion engine. In the former, the thrust is delivered in a single impulse, and in the latter, as in the case of the SOHR, the thrust acts continuously for a prescribed length of time. The specific impulse, I_{sp}, specific mass of the power plant, (α), and engine efficiency, η, assigned to the SOHR-SET and ion engines, are given in Table 1 along with the specific impulse for the chemical rocket. Here, $\alpha = M_w/P$, where M = mass of the propulsion power plant and does not include part of power plant used to generate electrical power for other than propulsion purposes. P = power delivered to rocket from power supply.

TABLE I

Engine Parameters

	SOHR-SET	Ion Engine	Chemical Rocket
I_{sp}	800 sec.	4000 sec.	400 sec.
α	4 lb/kw	40 lb/kw	---
η	0.70	0.63	---

The value of α given for the ion engine will, presumably, be achieved with the SNAP-50 power plant (300 kw system).

5.2 Analysis

In order to accomplish the desired mission of passing within three tenths of an Astronomical Unit from the sun, the probe must first escape from the earth. In the case of the chemical rocket, escape is realized simply by applying a single impulse to the probe, the impulse magnitude depending on the distance of the probe from the earth. In the case of the SOHR-SET or ion engine, the probe is first established (by chemical rocket) in an orbit about the earth, and then, under the action of low thrust, the probe slowly spirals out to escape, executing many revolutions about the earth, and taking a great deal of time in the process. In order to avoid the long computing times associated with this spiral motion, and the complexity introduced by the SOHR-SET passing through the earth's shadow, it is assumed that the probe has already escaped from the earth, and is describing a circular orbit about the sun at a radius of one astronomical unit (AU). Thus, the desired mission will be initiated from this circular orbit with the chemical rocket, as well as with the SOHR-SET and ion engine.

In the case of the chemical rocket, a single impulse is applied to the probe, in a direction opposite to its motion, such that the resulting ellipse has a perihelion distance equal to 0.30 AU. Refer to Fig. 5-1. The change in velocity required to produce this ellipse is ΔV = 31,300 ft/sec. If we assume that the vehicle is a single stage rocket, then the payload plus structure fraction delivered along the ellipse is

$$\frac{M_L + M_s}{M_o} = e^{-\frac{\Delta V}{I_{sp} g}} = 0.08716$$

where

M_L = payload
M_s = structure
M_o = initial mass of vehicle ($M_L + M_s + M_p$
M_p = total propellant.

The time taken to reach perihelion is 95.5 days, which is half the period of the ellipse.

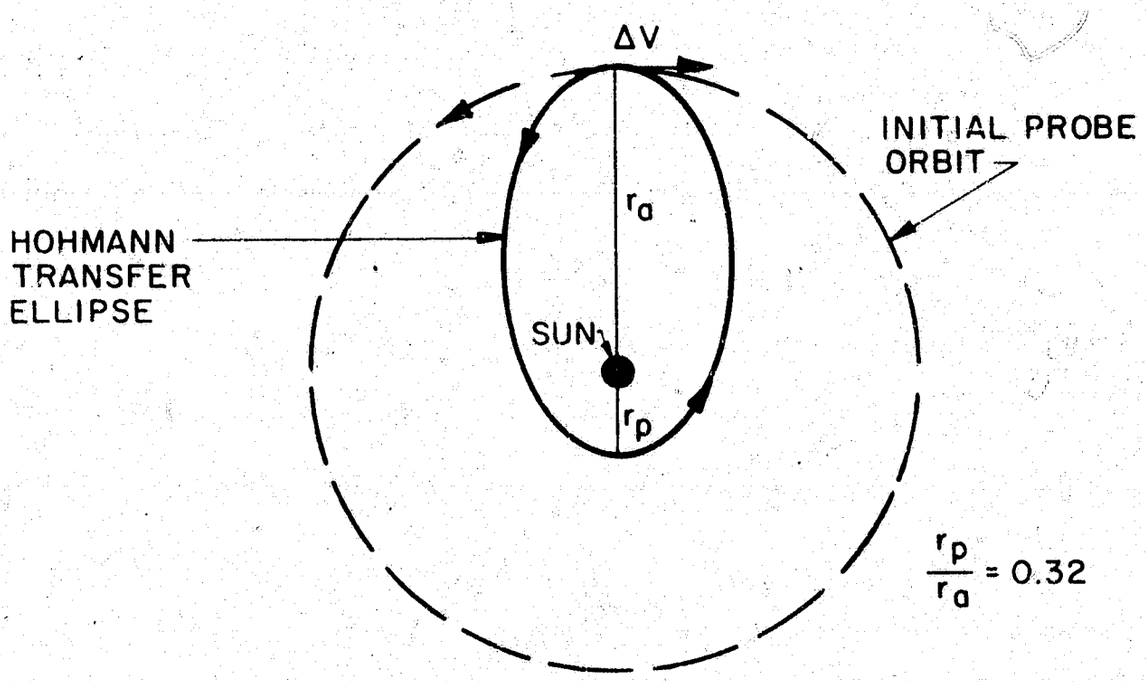

FIG. 5-1 HOHMANN TRANSFER ELLIPSE FOR CHEMICAL ROCKET

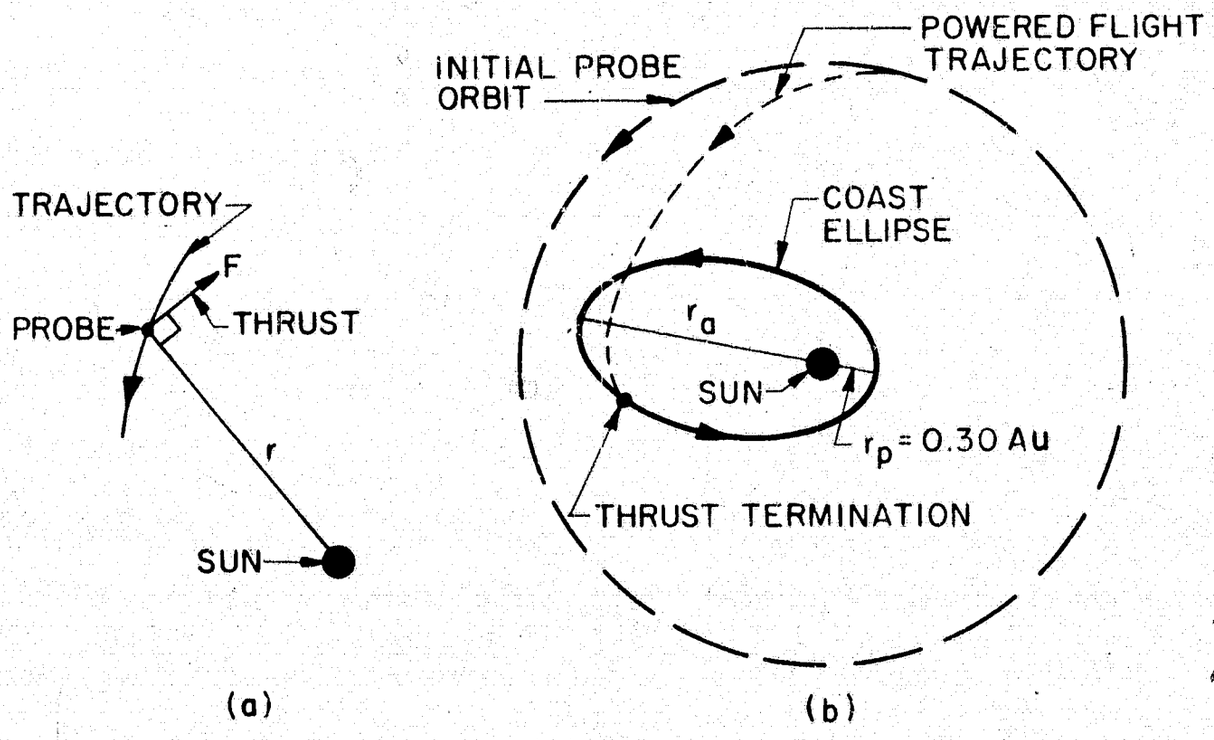

FIG. 5-2 COAST ELLIPSE FOR SOHR-SET AND ION ENGINE

In order for the SOHR-SET, or ion engine, propelled vehicle to fall toward the sun, energy must be removed from the initial orbit over an extended period of time. A simple and efficient way of removing this energy is to maintain the thrust in the plane of the initial orbit, perpendicular to the radius vector from the sun to the probe, in a direction opposite to the probe's motion, Refer to Fig. 5-2a. In order to minimize the expenditure of propellant, and thereby maximize the delivered payload, the thrust is terminated at the moment when the perihelion of the subsequent coast ellipse equals the desired 0.30 AU. Refer to Fig. 5-6. For constant thrust, i.e., constant propellant flow rate and constant specific impulse, the power supply and propellant fractions are given, respectively, as follows:

$$\frac{M_w}{M_o} = \frac{I\alpha}{46\eta g} \frac{F}{M_o} \qquad (5\text{-}1)$$

$$\frac{M_p}{M_o} = \frac{t_1}{I_{sp} g} \frac{F}{M_o} \qquad (5\text{-}2)$$

where F = thrust, t_1 = time of power flight, g = 32 ft/sec.^{2} The payload plus structure fraction is then

$$\frac{M_L + M_s}{M_o} = 1 - \frac{M_w}{M_o} - \frac{M_p}{M_o} \qquad (5\text{-}3)$$

If the SOHR-SET takes full advantage of the sun's radiation, then the power delivered by the solar concentrator to the engine will vary inversely as the square of the distance of the probe from the sun, i.e., $P \sim 1/r^2$. Since $F \sim P$, therefore $F \sim 1/r^2$, or,

$$F = F_o \frac{r_o^2}{r} \qquad (5\text{-}4)$$

where r_o = 1 AU. Since M_w remains constant during flight, $F = F_o (r/r_o)^2$. Hence, the power plant mass fraction is given by (5-1), where $\alpha = \alpha_o$, $F = F_o$.

The propellant mass fraction is

$$\frac{M_p}{M_o} = \frac{r_o^2}{Ig} \frac{F_o}{M_o} \int_o^{t_1} \frac{dt}{r^2} \qquad (5\text{-}5)$$

and the payload plus structure is given by (5-3), where M_p/M_o is now given by (5-5).

The equations of motion (in two dimensions of the probe in the gravitational field of the sun were programmed on an IBM 1620 computer. Trajectories were simulated for values of initial thrust acceleration, a_o, in the range, 10^{-5} g $\leq a_o \leq 10^{-3}$g. The method of propulsion (SOHR-SET or ion engine) was characterized by the parameters I_{sp} and α, the former appearing in the equations of motion, and the latter occuring only in equation (5-1). Constant thrust was used for both ion engine and SOHR-SET and variable thrust (equation 5-4) for the SOHR-SET. The initial conditions were the same for all trajectories, i.e., a circular orbit about the sun with radius equal to 1 AU.

Figures 5-3 and 5-4 show the time of powered flight and distance of the probe from the sun at the instant of thrust termination, respectively, as a function of a_o, for the above three engines. From Fig. 5-3 we see that for a given value of a_o, the powered flight time is longest for the ion engine and shortest for the SOHR-SET variable thrust, as to be expected. Figure 5-4 shows that the ion engine is closest to the sun, and the SOHR-SET variable thrust the farthest, at the instant of thrust termination, for a given value of a_o.

Figure 5-5 shows the power plant mass fraction as a function of initial thrust acceleration for the SOHR-SET and ion engines. The mass fraction for the ion engine equals unity at $a_o = 1.81\ (10^{-4})$g. The propellant mass fractions are shown in Fig. 5-6 along with that of the chemical rocket. Note that the chemical rocket consumes more propellant than either low thrust device, for $a_o > 10^{-5}$g.

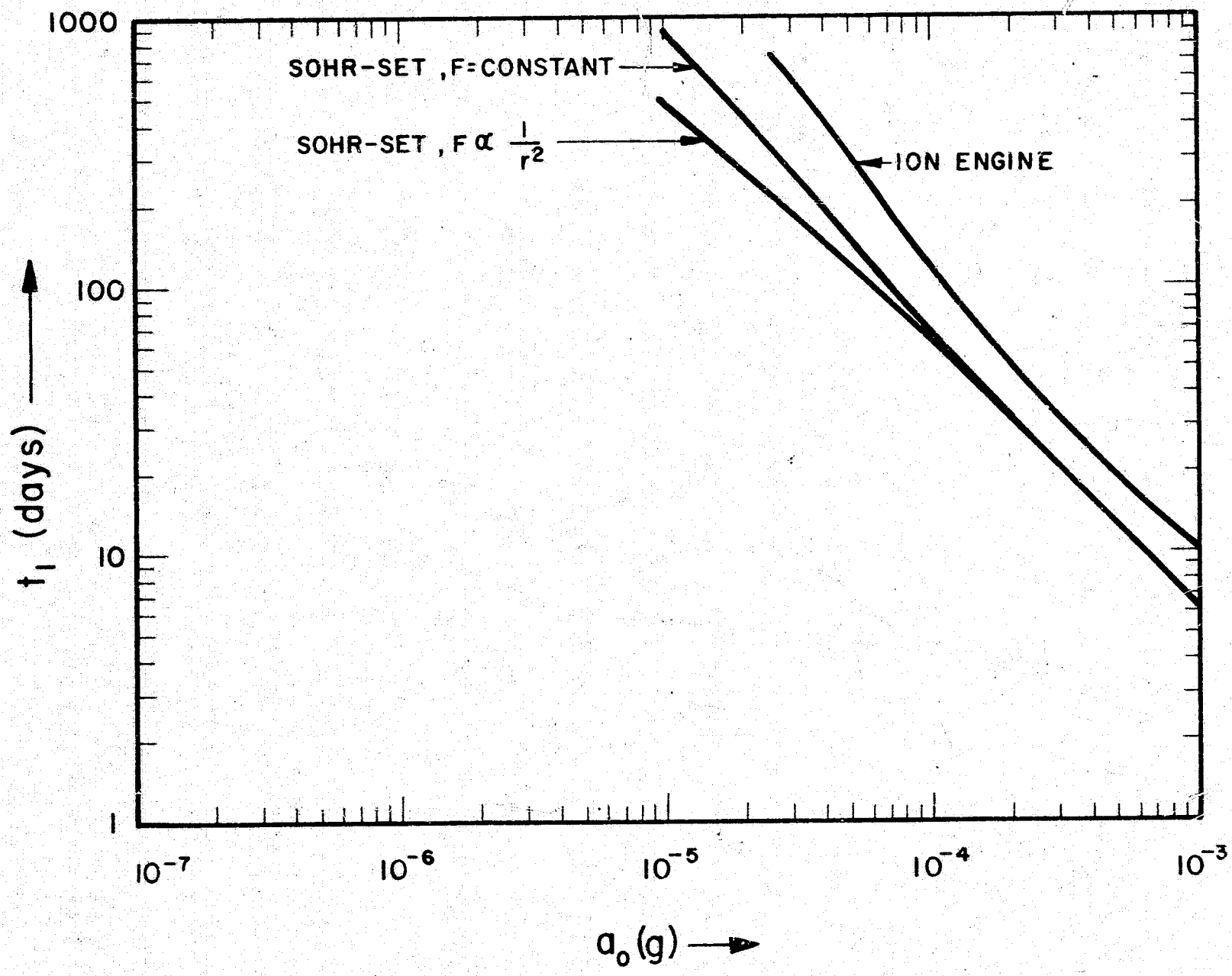

FIG. 5-3 TIME OF POWERED FLIGHT VS INITIAL THRUST ACCELERATION

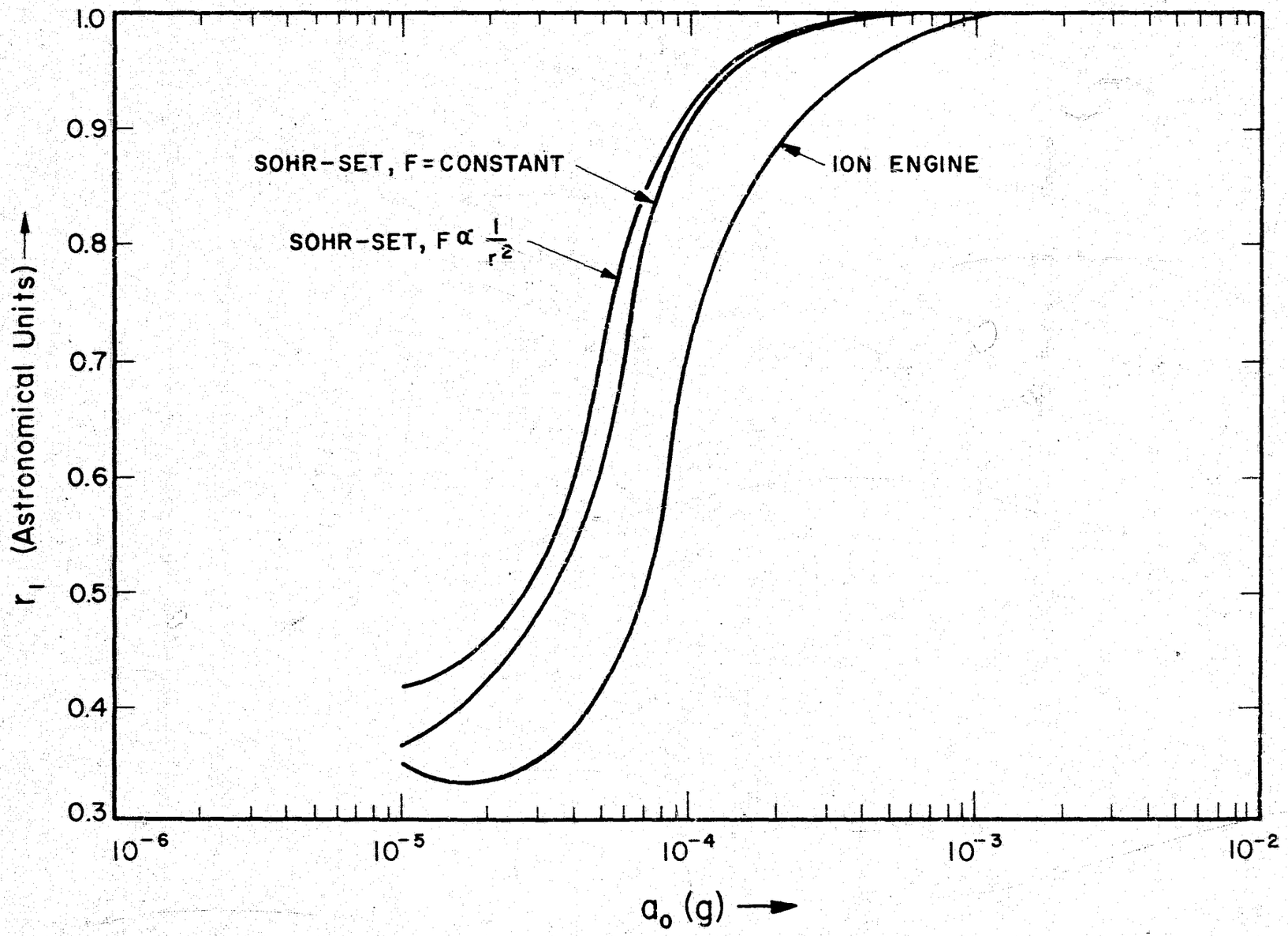

FIG. 5-4 DISTANCE FROM SUN AT INSTANT OF THRUST TERMINATION VS INITIAL THRUST ACCELERATION

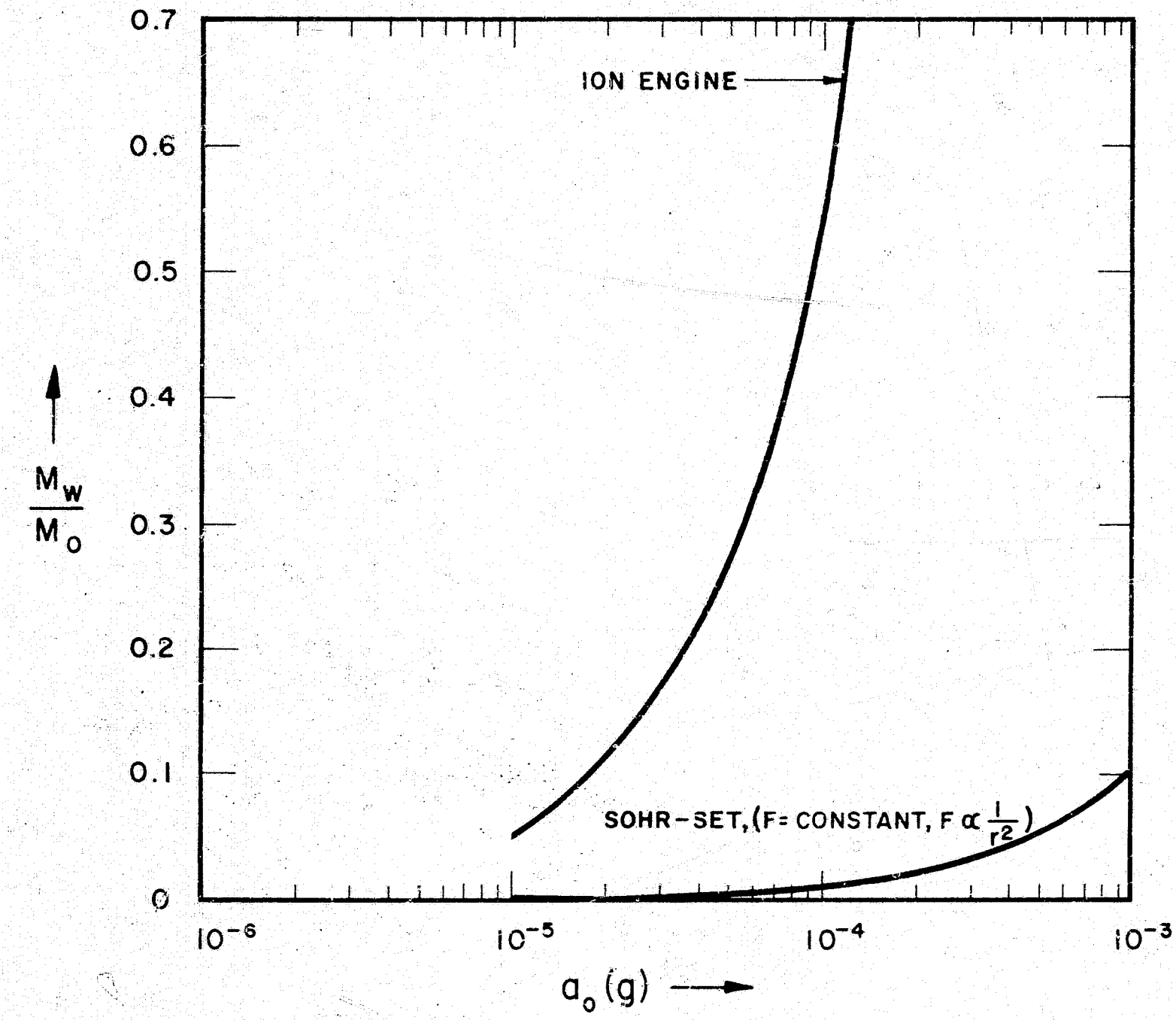

FIG. 5-5 POWER PLANT MASS FRACTION VS INITIAL THRUST ACCELERATION

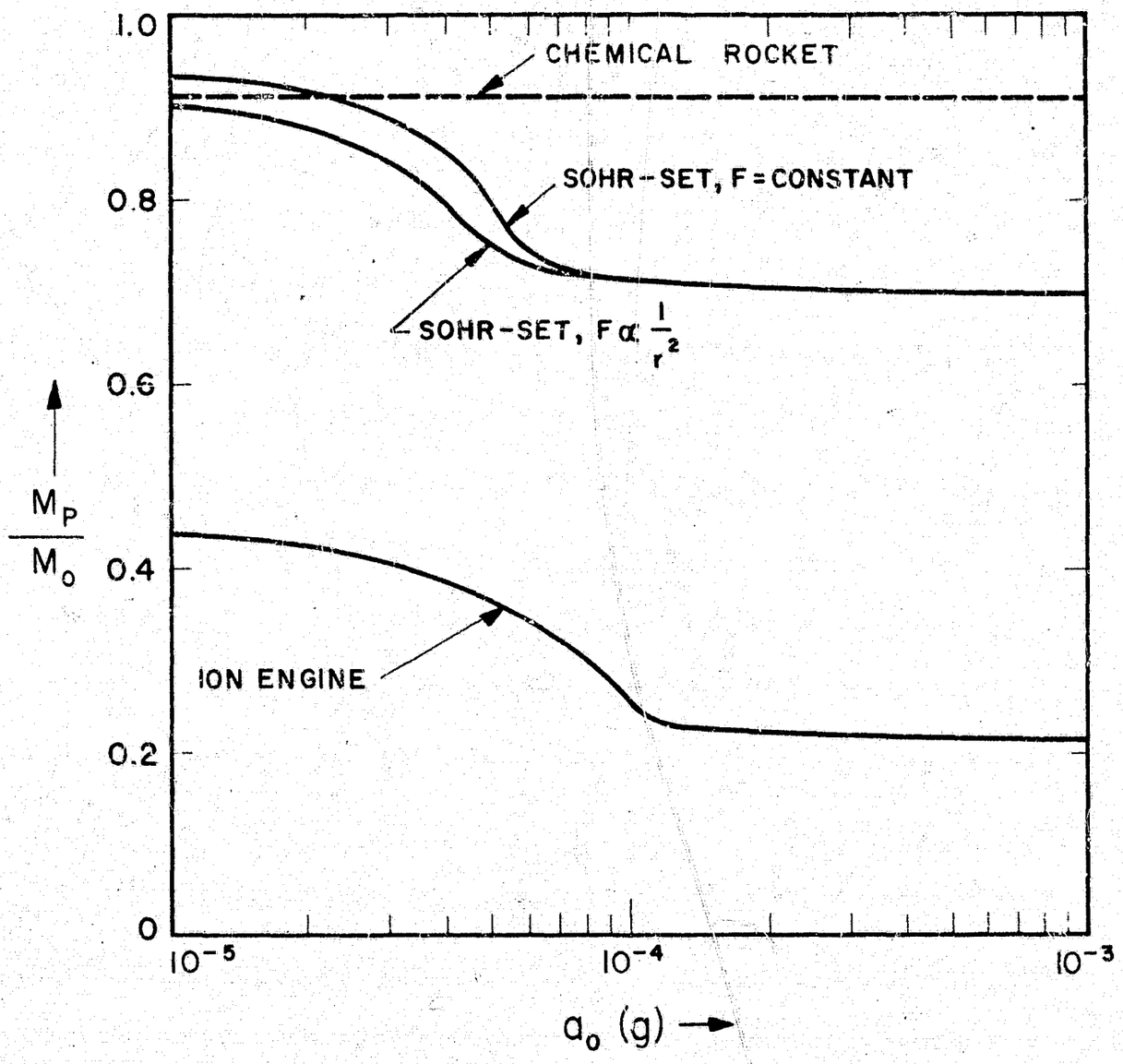

FIG. 5-6 PROPELLANT MASS FRACTION VS INITIAL THRUST ACCELERATION

Employing eq. (5-3), we obtain the payload (plus structure) mass fractions shown in Fig. 5-7. Since $M_w/M_o + M_p/M_o = 1$ at $a_o = 1.4\ (10^{-4})$ g for the ion engine, therefore the payload fraction is zero beyond this value of a_o. Judging from Fig. 5-7, the payload capability of the SOHR-SET is superior to the ion engine for large thrust accelerations, and inferior for small a_o, the crossover point being at approximately $a_o = 8(10^{-5})$ g. Note that the payload delivered by the SOHR variable thrust (eq. 5-4) is greater than that delivered by the SOHR constant thrust only for small values of a_o, i.e., $a_o < 10^{-4}$ g. The payload fraction for the chemical rocket is generally less than that of either the SOHR or ion engine.

Equally important as the delivered payload is the time required to perform the mission. The total mission time is the time of powered flight (Fig. 5-3) plus the time taken to go from the point of thrust termination to the perihelion of the coast ellipse (refer Fig. 5-2(b). Figure 5-8 shows the total mission time as a function of a_o for the three engines. Note that the mission times for the SOHR-SET are significantly less than those for the ion engine in the region $a_o < 10^{-4}$ g. However, this is the region in which the ion engine delivers the larger payload fraction. Clearly, a compromise must be made between payload and mission time.

Having established the probe in an elliptical orbit about the sun, it is of interest to know the properties of this orbit. Two important properties are the period (T) and aphelion (r_a) of the ellipse. These are shown in Figs. 5-9 and 5-10 respectively. From Fig. 5-10 we see that the probe will return to the earth's orbit ($r_a = 1$) only if the vehicle was propelled by the SOHR-SET at initial thrust accelerations exceeding $2(10^{-4})$ g.

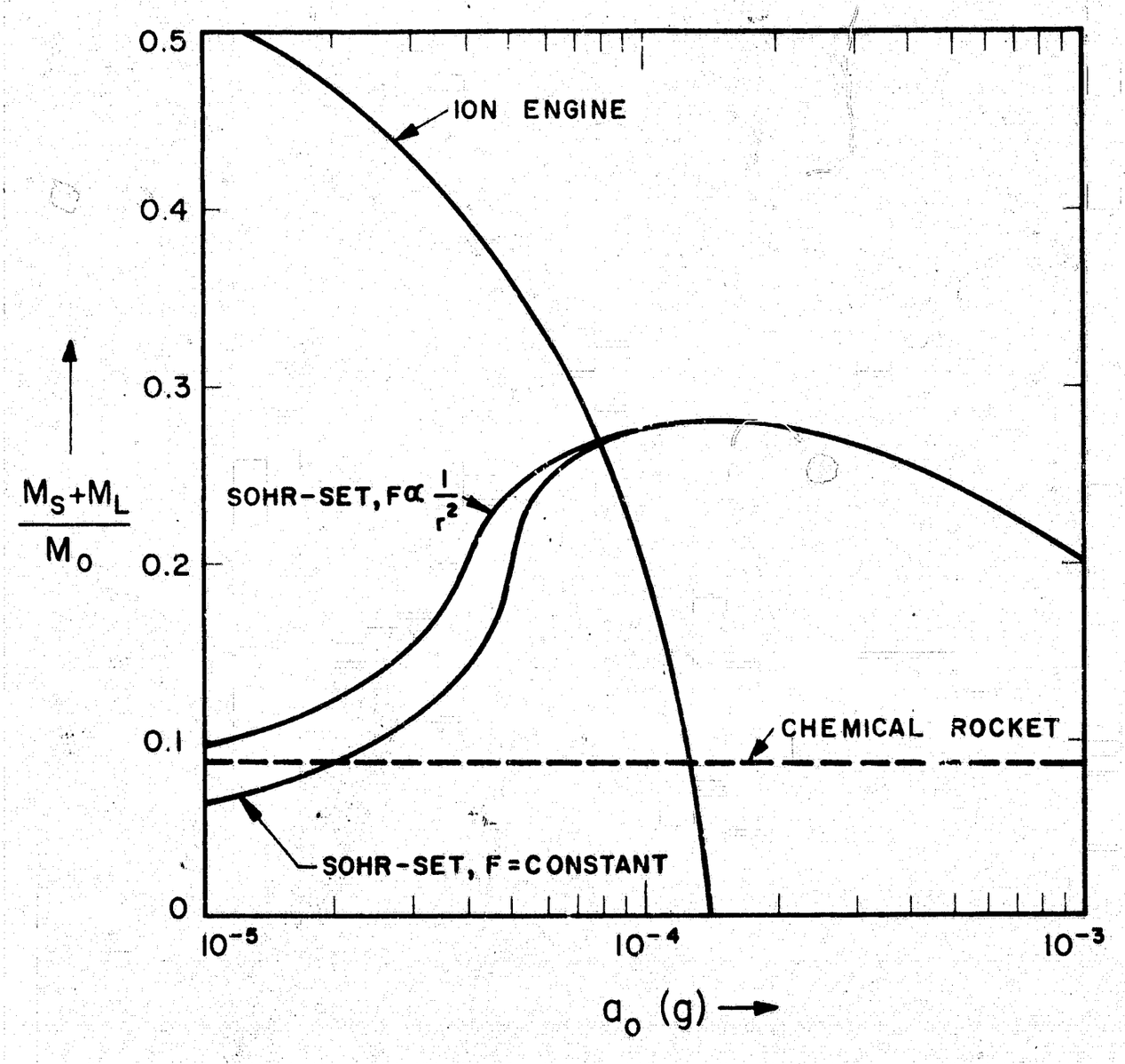

FIG. 5-7 PAYLOAD PLUS STRUCTURE MASS-FRACTION VS INITIAL THRUST ACCELERATION

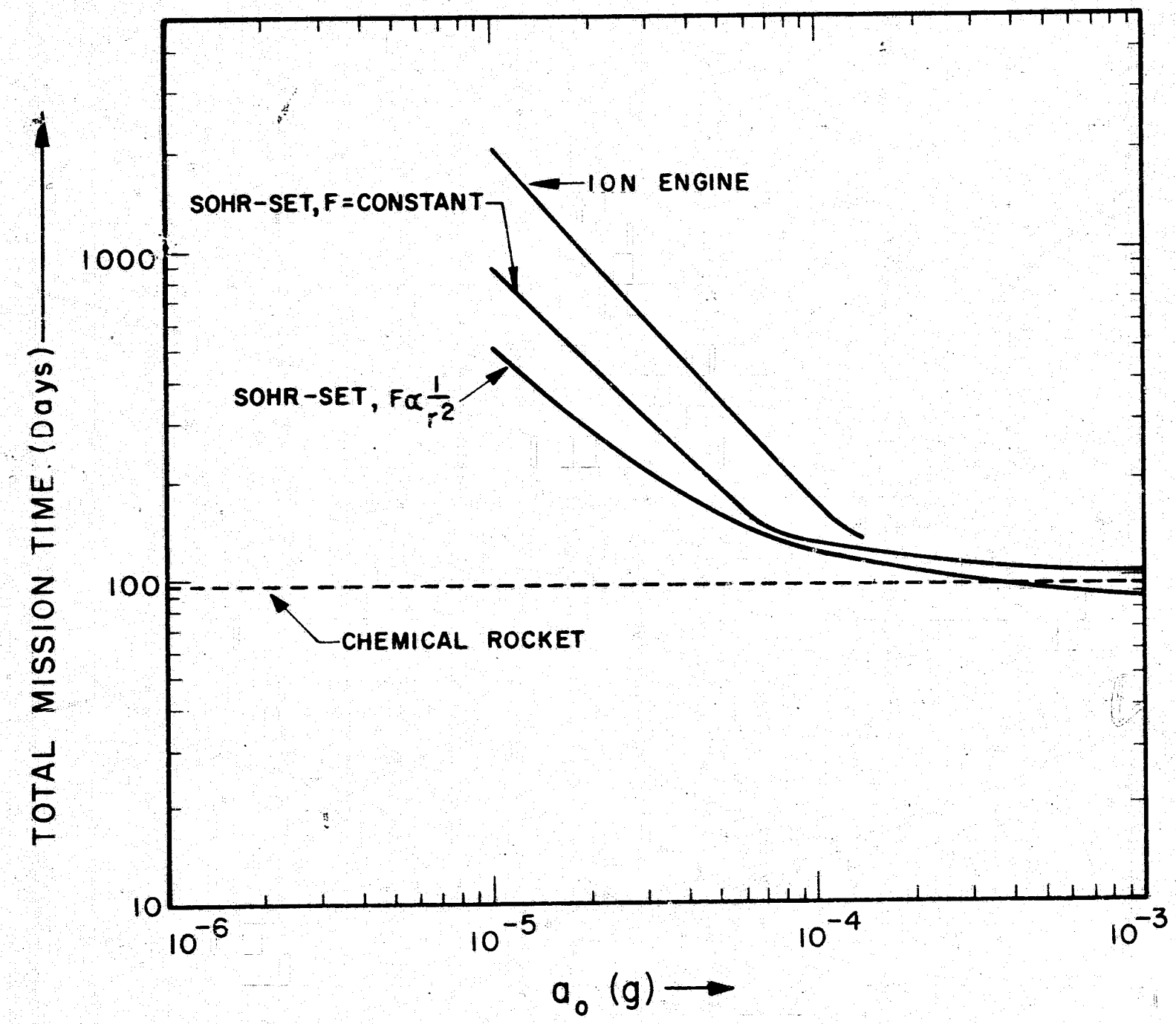

FIG. 5-8 TOTAL MISSION TIME VS INITIAL THRUST ACCELERATION

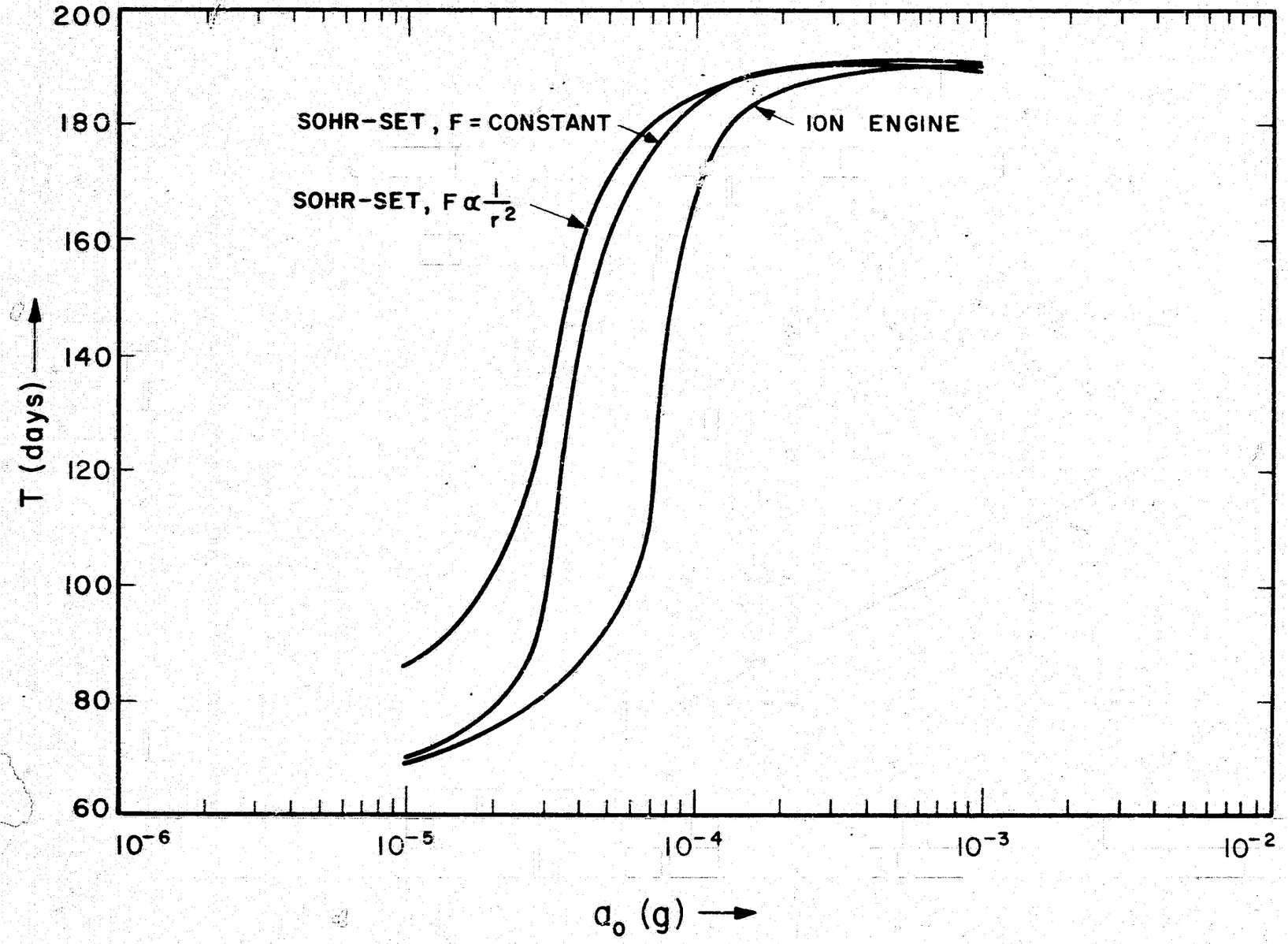

FIG. 5-9 PERIOD OF COAST ELLIPSE VS INITIAL THRUST ACCELERATION

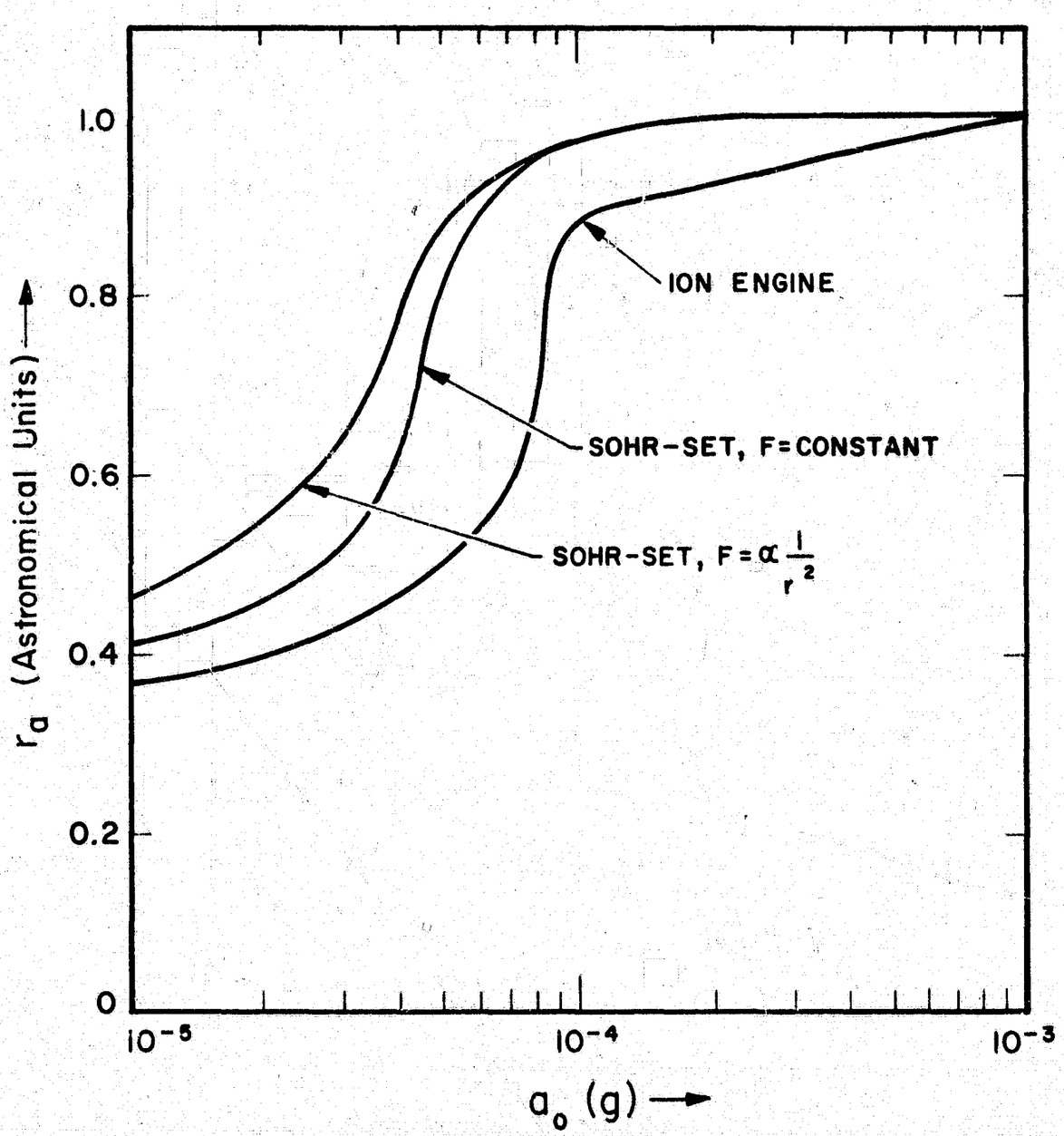

FIG. 5-10 APHELION DISTANCE OF COAST ELLIPSE VS INITIAL THRUST ACCELERATION

5.3 Conclusions

The SOHR-SET (defined in Table 1) is competitive with the ion engine (defined in Table 1) in both payload and mission time, for the solar probe mission. The ion engine cannot deliver a payload at initial thrust accelerations exceeding $a_o = 1.4 \times 10^{-4} g$ (refer Fig. 5-7), and although the payload fraction of the SOHR-SET is less than that of the ion engine for $a_o < 1.4 \times 10^{-4} g$. the mission times of the SOHR-SET are significantly less than those of the ion engine for this range of a_o. For thrust accelerations less than $10^{-4} g$, the variable thrust ($F \sim 1/r^2$) SOHR-SET delivers a greater payload and provides shorter mission times than the constant thrust SOHR, but the increase in payload is not as impressive as the decrease in mission time. Both ion engine and SOHR-SET are superior to the chemical rocket in "payload" capability, but are inferior in mission time. However, it should be noted that power requirements (excluding conditioning equipment) will be available at approximately 40 lb/kw for the SOHR-SET system and at 200 lb/kwe for the chemical system assuming solar-cells are used with the latter. Since the power conditioning equipment requirement will be approximately the same for both systems, the true payload advantage of the SOHR-SET will probably be even more favorable.

REFERENCES

1. ELECTRO-OPTICAL SYSTEMS, INC. Report-C17a-3C26.5. Research and Development Studies to Determine Feasibility of Solar LH_2 Propulsion System.
2. J. C. Evard: "How Much Future for Electric Propulsion?" Astronautics and Aerospace Engineering, August, 1963.
3. E. F. Batutis; "Storing Thermal Energy" Astronautics and Aerospace Engineering, May, 1963.
4. ELECTRO-OPTICAL SYSTEMS, INC. Report. 580 Final.